Role of conserved arginine in the heme distal site of HutZ from *Vibrio cholerae* in the heme degradation reaction

Takeshi Uchida[*a,b], Nobuhiko Dojun[a], Kazuki Ota[a], Yukari Sekine[a], Yuina Nakamura[a], Sayaka Umetsu[c] and Koichiro Ishimori [a,b]

[a]Department of Chemistry, Faculty of Science, Hokkaido University, Sapporo 060-0810, Japan

[b]Graduate School of Chemical Sciences and Engineering, Hokkaido University, Sapporo 060-8628, Japan

[c]Division of Chemistry, School of Science, Hokkaido University, Sapporo 060-0810, Japan

*Corresponding author: Department of Chemistry, Faculty of Science, Hokkaido University, Sapporo 060-0810, Japan

E-mail address: uchida@sci.hokudai.ac.jp (T. Uchida).

Keywords: heme, *Vibrio cholerae*, heme oxygenase, enzyme, reaction mechanism

ABSTRACT

HutZ from *Vibrio cholerae* is a dimeric enzyme that catalyzes degradation of heme. The highly conserved Arg92 residue in the HutZ family is proposed to interact with an iron-bound water molecule in the distal heme pocket. To clarify the specific role of Arg92 in the heme degradation reaction, the residue was substituted with alanine, leucine, histidine or lysine to modulate electrostatic interactions with iron-bound ligand. All four Arg92 mutants reacted with hydrogen peroxide to form verdoheme, a prominent intermediate in the heme degradation process. However, when ascorbic acid was used as an electron source, iron was not released even at pH 6.0 despite a decrease in the Soret band, indicating that non-enzymatic heme degradation occurred. Comparison of the rates of heme reduction, ligand binding and verdoheme formation suggested that proton transfer to the reduced oxyferrous heme, a potential rate-limiting step of heme degradation in HutZ, is hampered by mutation. In our previous study, we found that the increase in the distance between heme and Trp109 from 16 to 18 Å upon lowering the pH from 8.0 to 6.0 leads to activation of ascorbic acid-assisted heme degradation by HutZ. The distance in Arg92 mutants was >19 Å at pH 6.0, suggesting that subunit-subunit interactions at this pH are not suitable for heme degradation, similar to Asp132 and His63 mutants. These results suggest that interactions of Arg92 with heme-bound ligand induce alterations in the distance between subunits, which plays a key role in controlling the heme degradation activity of HutZ.

1. Introduction

Almost all bacteria require iron for survival and have developed sophisticated mechanisms to solubilize, sequester and release iron within the cell. Most bacterial pathogens have evolved to take advantage of heme-containing proteins as a source of iron. The ability to transport and utilize heme is a common mechanism employed by pathogenic bacteria to establish and maintain infection [1–6]. Exogenously acquired heme is oxidized to release iron by heme-degrading enzymes for utilization by bacteria.

Based on the genome sequence of *Vibrio cholerae* and bioinformatics-based predictions, putative genes encoding heme acquisition have been identified, termed *hut* (heme utilization) [7–9]. The Hut protein family includes outer membrane heme transport proteins (HutA and HutR) [10–12], inner membrane heme transport proteins (HutC/HutD) and heme carrier proteins (HutB and HutX) [13,14]. HutZ was previously identified as a heme-degrading enzyme by our group [15]. HutZ can cleave heme to biliverdin *via* verdoheme, similar to the mechanism used by human heme oxygenase (hHO). However, the cleavage site is in the β- or δ-meso and not the α-meso position, as observed for HO [15]. An interesting feature of HutZ is the extremely slow reaction rate at neutral or alkaline pH [15]. Specifically, the reaction rate above pH 7.0 is significantly slower than that at pH 6.0.

Although the X-ray crystal structure of HutZ in the heme-bound form is not available, resonance Raman data suggest that the heme environment has an unusual structure [15]. The plots of Fe-CO ($\nu_{Fe\text{-}CO}$) and C-O ($\nu_{C\text{-}O}$) stretching modes of the CO-bound form are far off from the line with proteins possessing neutral histidine as an axial ligand but near the line with proteins with imidazolate as the axial ligand. The imidazolate character of the proximal histidine with negative redox potential of heme from heme-HutZ at pH 8.0 (–176 mV) leads to stabilization of ferric rather than ferrous heme, resulting in a slow reduction rate of heme [16]. In addition, even if heme is reduced, oxyferrous heme is rapidly re-oxidized to ferric

heme via autoxidation. The half-life of the oxyferrous heme of HutZ at pH 8.0 is less than 10 s [15], whereas that of heme-HO is more than 1 h [17]. Accordingly, almost no heme degradation occurs in heme-HutZ at pH values of 7.0 or above [16]. In contrast, the heme iron at pH 6.0 is reduced faster relative to that under neutral or alkaline conditions by ~3-fold, potentially due to lower electron donation from proximal histidine [16]. Thus, heme in the heme-HutZ complex is efficiently degraded at pH 6.0 but not pH >7.0.

The structure of apo-HutZ was solved and its docking structure of heme predicted that Arg92 and His63 coordinate heme [18]. However, the results of our mutational studies suggested that His170 is a sole heme ligand, which was not coincident with the docking model [19,20]. The crystal structure of a HutZ homologous protein HugZ from *Helicobacter pylori* suggests that His170 of HutZ is the proximal heme ligand, which is within hydrogen bonding distance of Asp132 (Fig. 1). The hydrogen bond between Asp132 and His170 could contribute to the imidazolate characteristic of proximal His170, as observed for most peroxidases [21–23]. To validate the importance of the proximal hydrogen bond in the heme degradation reaction, Asp132 or His170 was substituted in a previous study by our group [20]. Notably, disruption of the hydrogen bond between His170 and Asp132 did not affect enzymatic activity whereas this bond was necessary for heme positioning into the appropriate position for degradation.

The Fe-CO stretching mode of CO-bound heme ($\nu_{Fe\text{-}CO}$) is also known as a sensitive marker of electrostatic conditions within the distal heme pocket [24–27] and observed at 504 cm^{-1} for heme-HutZ [15]. This frequency is almost identical to that of myoglobin [28], indicating the involvement of strong positive electrostatic interactions between iron-bound CO and distal residues in heme-HutZ. The absorption spectrum of ferric heme-WT HutZ is typical of six-coordinate low-spin heme, suggestive of binding of OH^- ion to heme [15]. In contrast, the protonated Fe^{3+}-H_2O form (high spin) was dominant at acidic pH. Heme degradation activity was also pH-dependent; HutZ is active at pH 6.0, but it is inactive at pH

>7.0 [16]. In view of the correlation between the high-spin heme content and heme degradation activity, we propose that heme degradation activity of HutZ is related to the high-spin heme content [16].

The high-spin to low-spin heme ratio is associated with distal amino acid residues. Arg166 of HugZ from *H. pylori*, a highly conserved residue, interacts with an iron-bound azide ligand [29]. Comparison of amino acid sequences led to the prediction that Arg92 of HutZ from *V. cholerae* corresponds to Arg166 of HugZ. Considering the prediction that Arg92 is located near the iron-bound ligand in the crystal structure of HugZ, the residue at this position is postulated to stabilize the Fe^{3+}-OH^- form (low spin) through electrostatic interactions under neutral or alkaline pH, leading to enhancement of proximal hydrogen bonding between His170 and Asp132 and decrease in heme degradation activity. In general, arginine is not an effective residue as a catalytic center owing to its high pK_a value. In most heme peroxidases, histidine in the heme distal side acts as an acid-base catalyst [30]. In contrast, in hHO, distal glycine is important for oxidation of the heme macrocycle and suppression of peroxidase activity [31,32]. Based on these results, we hypothesize that Arg92 of HutZ plays an important role in the heme degradation reaction.

To clarify the activation mechanism of HutZ and the role of conserved distal arginine, we generated four Arg92 mutant enzymes (R92A, R92L, R92H and R92K) in this study. Arg92 appeared necessary for heme degradation when ascorbic acid was used as the electron donor, since almost no iron was released from heme after reaction with ascorbic acid. Considering that the mutants converted heme to verdoheme in the reaction with hydrogen peroxide (H_2O_2), Arg92 may play a key role in transferring H^+ to a heme degradation intermediate, Fe^{3+}-OO^-, presumed to be a rate-limiting step of heme degradation by HutZ [33]. In contrast to hHO, HutZ is a dimeric protein. Recent studies by our group further showed that subunit-subunit interactions play a key role in the heme degradation reaction [16]. The distance between heme and Trp109, which reflects subunit-subunit orientational changes, was increased from 16–18

Å for wild-type HutZ to 23-25 Å for R92A and R92L mutant enzymes, similar to data obtained for mutants of Ala31 [16], His63 [19] and Asp132. Based on the collective results, we propose an activation mechanism of HutZ involving conformational changes at Arg92, which are transmitted to the heme axial ligand His170 through Ala31, His63, and Asp132, with modulation of subunit-subunit interactions.

2. Experimental section

2.1. Materials

Chemicals were purchased from Wako Pure Chemical Industries (Osaka, Japan), Nacalai Tesque (Kyoto, Japan) or Sigma-Aldrich (St. Louis, MO, USA) and used without further purification.

2.2. Protein preparation

Mutant HutZ proteins were expressed in *Escherichia coli* and purified as described previously [20]. Mutagenesis was conducted utilizing a PrimeSTAR mutagenesis basal kit from Takara Bio (Otsu, Japan). DNA oligonucleotides were purchased from Eurofins Genomics (Tokyo, Japan). The primers employed for mutation are listed in Supplemental Table 1. Genes were sequenced (Eurofins Genomics) to ensure that only the desired mutations were introduced. The protein concentration of HutZ was determined based on absorbance at 280 nm. A molar extinction coefficient (ε_{280}) of 9.97 $mM^{-1}cm^{-1}$ was obtained using the ProtParam server (http://web.expasy.org/protparam/).

2.3. Measurement of heme binding to HutZ

Heme binding was monitored using difference spectra in the Soret region of the UV-visible spectrum. Hemin was dissolved in 0.1 M NaOH and its concentration determined based on absorbance at 385 nm using an extinction coefficient (ε_{385}) of 58.44 mM^{-1} cm^{-1} [34]. Successive aliquots of 0.5 mM hemin in NaOH (pH ~13) were added to both the sample

cuvette containing 10 μM apo-HutZ in 50 mM Tris-HCl and 150 mM NaCl (pH 8.0) and reference cuvette. Spectra were recorded 3 min after the addition of each heme aliquot. No pH changes in the medium were observed after the addition of hemin solution. Absorbance differences at 404-409 nm were plotted as a function of heme concentration, and apparent dissociation constants ($K_{d,heme}$) calculated using a quadratic binding equation [35].

2.4. Spectroscopy

Optical spectra of purified proteins were recorded using a V-660 UV-visible spectrophotometer (Jasco, Tokyo, Japan) at 25 °C. pH titration of heme-reconstituted HutZ in the ferric form was conducted based on absorption spectra. The pH was altered by the addition of small amounts of 1 N HCl to protein solution in 50 mM sodium phosphate or borate buffer, and actual pH values measured with a micro pH electrode (Horiba, Kyoto, Japan). Determination of pK_a values was performed by curve fitting of the fraction of the alkaline form versus pH for the given pH values in the Henderson-Hasselbalch equation.

Resonance Raman spectra were obtained with a single monochromator (SPEX500M, Jobin Yvon, Edison, NJ, USA) equipped with a liquid nitrogen-cooled CCD detector (Spec-10:400B/LN, Roper Scientific, Princeton, NJ, USA). The excitation wavelengths employed were 413.1 and 441.6 nm from a krypton ion (BeamLok 2060, Spectra Physics, Santa Clara, CA) and helium-cadmium (IK5651R, Kimmon Koha, Tokyo, Japan) lasers, respectively. The laser power at the sample point was adjusted to ~5 mW for ferric and ferrous forms and 0.1 mW for the CO-bound form to prevent photodissociation. Raman shifts were calibrated with indene, CCl_4, acetone, and an aqueous solution of ferrocyanide. The accuracy of the peak positions of well-defined Raman bands was ±1 cm^{-1}. Samples for resonance Raman experiments were prepared at a concentration of ~10 μM in 50 mM Tris-HCl and 150 mM NaCl (pH 8.0).

Fluorescence spectra were recorded using a FP-8500 spectrometer (Jasco). Protein samples

were excited at 295 nm to avoid contribution from tyrosine residues. The sample concentration was 10 μM in 50 mM Tris-HCl and 150 mM NaCl (pH 8.0). The distance (r) between tryptophan and heme was estimated based on the efficiency (E) of Förster energy transfer from tryptophan to heme, defined as:

$$E = \frac{R_0^6}{R_0^6 + r^6} \quad (1)$$

whereby R_0 represents the Förster distance and R_0 for heme and tryptophan is 29 Å [36]. The energy transfer efficiency, E, was calculated using the fluorescence intensity of apo-HutZ (F_{apo}) and heme-HutZ (F_{heme}) as follows:

$$E = \frac{F_{apo} - F_{heme}}{F_{apo}} \quad (2)$$

2.5. Heme degradation activity

The heme degradation reaction of HutZ was monitored via spectrophotometry. Briefly, 1.9 mL hemin-reconstituted protein solution (final concentration, 10 μM) in 50 mM Tris-HCl and 150 mM NaCl (pH 8.0) was placed in a cuvette and the reaction initiated by adding 100 μl of 4 mM H_2O_2 or 20 mM ascorbic acid in the same buffer at 25 °C. Spectra were recorded at 1 min intervals for 15 min for H_2O_2 and 2 min intervals for 60 min for ascorbic acid. In the case of reactions with ascorbic acid (final concentration, 1 mM), 1 mg mL^{-1} of bovine liver catalase was added to suppress H_2O_2. After completion of the reaction, ferrozine (Dojindo, Kumamoto, Japan) was added to a final concentration of 1 mM. The amount of released iron was calculated by measuring absorbance at 562 nm using an extinction coefficient (ε_{562}) of 27.9 $mM^{-1}cm^{-1}$ [37].

Kinetic analyses of verdoheme formation were performed using a stopped-flow apparatus (Unisoku, Osaka, Japan). The reaction was monitored immediately after mixing equal volumes of 10 μM HutZ (50 mM Tris-HCl and 150 mM NaCl, pH 8.0) and 200 μM H_2O_2. Decay of absorbance at 644-647 nm was fitted using a single exponential equation.

2.6. Reduction of heme

The reduction rate of heme, k_{red}, was determined by monitoring changes in absorbance at 418 nm. Ferric heme-HutZ (5 μM) was reduced using 1 mM ascorbic acid. Although an oxygen scavenging system composed of glucose, glucose oxidase and catalase was added to the solution to maintain anaerobiosis [38], the reaction was conducted under a carbon monoxide (CO) atmosphere to prevent oxidative cleavage of heme and/or autoxidation by contaminated O_2. The k_{red} values were obtained by fitting the time-course of absorbance change to a single or double exponential equation.

2.7. Cyanide binding rate constants

Cyanide ion (CN) binding to heme was measured by following the decrease in absorbance at 412 nm using stopped-flow apparatus (Unisoku). In a typical CN binding experiment, one syringe contained 5 μM HutZ (50 mM Tris-HCl and 150 mM NaCl, pH 8.0) and another contained at least 100-fold excess CN. Three determinations were performed for each ligand concentration. The mean of the pseudo-first-order rate constant, k_{obs}, was used to calculate the second-order rate constants obtained from the slope of a plot of k_{obs} versus ligand concentration ($k_{obs} = k_{on}[CN] + k_{off}$).

3. Results

3.1. Heme binding properties of Arg92 mutants

Four Arg92 mutants (R92A, R92L, R92H and R92K) were purified using the same procedure as wild-type (WT) HutZ. Titration of heme into mutant proteins was conducted by monitoring spectral changes at 404-409 nm (Fig. 2, insets). The apparent dissociation constants ($K_{d,heme}$) of R92A, R92L, R92H and R92K mutants for heme were estimated as 0.26 ± 0.02, 1.01 ± 0.25, 0.46 ± 0.06, and 0.029 ± 0.006 μM, respectively. Compared with WT HutZ (0.052 ± 0.004 μM) [15], all mutants of Arg92, except R92K, showed slightly reduced affinity for heme.

3.2. Spectroscopic characterization of heme-Arg92 mutant complexes

Absorption spectra of the Arg92 mutants reconstituted with equimolar hemin are shown in Fig. 2. The Soret peak of all four mutants in the ferric form at pH 8.0 showed a blue shift by 4–5 nm (Fig. 2, red lines), compared with heme-WT HutZ (412 nm) [15], suggesting increased six-coordinate high-spin heme at the expense of the six-coordinate low-spin heme. Although previous studies have reported that mutation of Arg92 to alanine does not affect the Soret peak [39], we clearly observed blue shifts for all four Arg92 mutants, indicative of changes in the interactions between the residue at position 92 and heme-bound water molecules. Upon lowering the pH from 8.0 to 6.0, a further blue shift of the Soret band to 406 nm was detected in all Arg92 mutants (Fig. 2, blue line), which was almost at the same position as that of heme-WT HutZ at pH 6.0 (Fig. 2A). As reported previously, pH dependence of UV-vis absorption spectra is explained by ionization of water molecule coordinated to the heme iron [15,28,40]. The pK_a values of equilibrium between the Fe^{3+}-H_2O (high spin) and Fe^{3+}-OH^- (low spin) forms for heme-R92A, heme-R92L, heme-R92H and heme-R92K mutants were estimated as 8.8, 8.7, 8.2, and 7.9, respectively (Supplemental Fig. S1), which were ~2–3 pH units higher than that of heme-WT HutZ [15]. The significant shift in pK_a values for Arg92 mutants demonstrated the involvement of Arg92 in acid-alkaline transition of the heme-bound water molecule. Although earlier data from a docking model of heme and apo-HutZ and mutational studies suggest that His63 and Arg92 are heme ligands, the changes in pK_a values between high-spin and low-spin heme observed due to mutation of Arg92 indicate that Arg92 is not a heme ligand but interacts with heme-bound water molecule [39].

Resonance Raman spectra of the heme-Arg92 mutants in the ferric state are shown in Fig. 3A. A spin-state marker band [41], ν_3, of the ferric heme-R92K mutant appeared at 1502 cm^{-1}, characteristic of the six-coordinate low-spin heme, similar to that observed for heme-WT HutZ [15]. For the heme-R92H mutant, the ν_3 band was composed of two bands with roughly

equal intensities at 1479 and 1503 cm^{-1} corresponding to six-coordinate high-spin and low-spin heme, respectively [41]. Resonance Raman spectra of the heme-R92A and heme-R92L mutants closely resembled each other. The ν_3 band of ferric heme-R92A and heme-R92L mutants contained three bands at 1481, 1488, and 1503 cm^{-1}, which were derived from the six-coordinate high-spin, five-coordinate high-spin and six-coordinate low-spin heme, respectively. The appearance of the five-coordinate species in the heme-R92A and heme-R92L mutants indicates that the electrostatic interactions involving the positive charge at position 92 contribute to stabilization of the coordinated water molecule to heme.

The frequencies of ν_2 bands also reflect the spin state of heme [41]. The bands at 1558 and 1582 cm^{-1} for heme-WT HutZ corresponded to six-coordinate high-spin and low-spin heme, respectively (Fig. 3A). In contrast to heme-WT HutZ, the absorbance of the former band was larger than that of the latter one in the heme-R92A, R92L and R92H mutants, indicating that high-spin heme is dominant in these mutants, as observed in the ν_3 bands (Fig. 3A) and absorption spectra (Fig. 2). Although ν_2 band of five-coordinate high-spin heme appears at ~1570 cm^{-1} in general [41], it was not assigned in the spectra of heme-WT and Arg92 mutant HutZ due to overlap with the 1558 and 1582 cm^{-1} bands.

Resonance Raman spectra of the ferrous five-coordinate species with histidine coordination revealed the Fe-His stretching mode, $\nu_{Fe\text{-}His}$, at 200-250 cm^{-1} [42]. The $\nu_{Fe\text{-}His}$ modes of heme-R92A, heme-R92L, heme-R92H and heme-R92K mutants were observed at 225–227 cm^{-1} (Fig. 3B), which were almost identical to that of heme-WT HutZ [15]. These frequencies indicate that mutation of Arg92 barely affects the Fe-His stretching mode of ferrous heme.

Resonance Raman spectra of the CO-bound heme-Arg92 mutants in the low frequency region are shown in Fig. 3C. For heme-R92H and heme-R92K mutants, a broad band was observed at 505 cm^{-1}. Upon substitution with $^{13}C^{18}O$, this band for heme-WT HutZ shifted to

498 cm^{-1} and was thus assigned to the Fe-CO stretching mode ($\nu_{Fe\text{-}CO}$) [15]. The frequencies of $\nu_{Fe\text{-}CO}$ for heme-R92H and heme-R92K mutants were roughly similar to that for heme-WT HutZ whereas $\nu_{Fe\text{-}CO}$ for heme-R92A and heme-R92L mutants was downshifted to 497–498 cm^{-1} [15]. The C-O stretching modes ($\nu_{C\text{-}O}$) for heme-R92A, heme-R92L, heme-R92H and heme-R92K mutants were observed at 1955, 1961, 1941 and 1936 cm^{-1}, respectively (Fig. 3D). Correlation plots of $\nu_{Fe\text{-}CO}$ and $\nu_{C\text{-}O}$ for heme-WT enzyme indicated that these modes were relatively uncorrelated for proteins with histidine as a heme ligand but correlated for proteins with imidazolate [15]. The correlation plots of $\nu_{Fe\text{-}CO}$ and $\nu_{C\text{-}O}$ for the heme-R92K, heme-R92L, heme-R92A and heme-R92H mutants moved towards the line of proteins with histidine as a heme ligand in this order (Fig. 3E). Although the signal-to-noise ratio of the Raman spectra in the high-frequency region was relatively low (Fig. 3D), the Raman spectra of the Arg92 mutants support the idea that arginine at position 92 is essential for the imidazolate character of the proximal histidine.

3.3. Heme degradation reaction of heme-Arg92 mutants at pH 8.0

Heme degradation activity was examined using ascorbic acid as an electron donor since the native electron donor of HutZ is unknown. The reaction was performed in the presence of catalase that scavenges H_2O_2 generated by direct reaction of ascorbic acid with molecular oxygen. Spectral changes after the addition of 1 mM ascorbic acid at pH 8.0 are shown in Fig. 4. Addition of ascorbic acid to Heme-Arg92 mutants at pH 8.0 led to a decrease in the Soret band, supporting the possibility that Arg92 mutants degrade heme even at pH 8.0. Thus, to monitor the amount of Fe^{2+} released from heme, ferrozine, which forms a complex with Fe^{2+} and displays strong absorption peaking at 562 nm [37], was added to the reaction solution. Notably, no absorption peak at 562 nm was evident, indicating that Fe^{2+} is not released from heme in the reaction with ascorbic acid at pH 8.0 (Fig. 4, green lines). Decrease in the Soret band without peak shift suggests that the porphyrin macrocycle is partially broken but Fe^{2+} is still attached to it. Loss of the Soret band without iron release was also encountered in

mutants of Ala31 to valine or leucine [16], indicating changes in subunit-subunit interactions as discussed below.

To confirm whether mutation of Arg92 resulted in loss of heme degradation ability, reactions with hydrogen peroxide (H_2O_2) were conducted. Fig. 5 shows the absorption spectral changes during reaction with H_2O_2. Absorption at ~644 nm derived from Fe^{3+}-verdoheme [33] increased in parallel with loss of the Soret band, suggesting that verdoheme is produced in the reaction with H_2O_2. To compare the reaction rates of the Arg92 mutants with H_2O_2, the time-courses of absorption changes at 646–648 nm in the reaction of 5 μM HutZ with 0.1 mM H_2O_2 were measured and rate constants (k_{verdo}) obtained by fitting the data with a single exponential curve (Fig. 5, insets). The apparent kinetic constants obtained for heme-R92A, heme-R92L, heme-R92H and heme-R92K mutants were 3.5 ± 0.6, 2.7 ± 0.5, 3.2 ± 0.4 and 0.70 ± 0.05 min^{-1}, respectively, which are 1.3–6.4-fold faster than that of heme-WT HutZ (0.55 ± 0.09 min^{-1}; Table 1), probably owing to the increase in Fe^{3+}-H_2O species (Fig. 2). We conclude that Arg92 mutants retain H_2O_2-dependent heme degradation ability.

3.4. Heme degradation activity of heme-Arg92 mutants at pH 6.0

The heme degradation reaction was additionally examined at pH 6.0, since the activity of the heme-WT enzyme on ascorbic acid is pH dependent. Heme-WT HutZ is active at pH 6.0 but inactive at pH 7.0 or higher [15,16]. UV-vis absorption spectral changes after addition of ascorbic acid at pH 6.0 are shown in Fig. 6. Absorption of the Soret band of heme-WT HutZ was diminished with a slight increase in absorbance in the visible region, as reported earlier [15], whereas only slight spectral changes were observed for heme-R92A, heme-R92L, and heme-R92H ~~and heme-R92K~~ mutants. The Soret band of the heme-R92K mutant was about half of the initial height. However, addition of ferrozine confirmed that Fe^{2+} was not released (Fig. 6E, green line), as observed at pH 8.0 (Fig. 4D). The decrease in the Soret band of the

R92K mutant suggests that heme was broken, but iron is held by the broken heme macrocycle. Thus, Fe^{2+} was not released from Arg92 mutants in the reaction with ascorbic acid at pH 6.0, in clear contrast to WT HutZ.

To confirm whether the mutants retain heme degradation ability at pH 6.0, reaction of the heme-Arg92 mutants with H_2O_2 was monitored. Spectral changes after the addition of H_2O_2 to heme-R92A, heme-R92L, heme-R92H and heme-R92K mutants at pH 6.0 are shown in Fig. 7. For all Arg92 mutants, absorption of the Soret band decreased rapidly with an increase in absorption at 645–648 nm, suggestive of verdoheme formation [33], as observed at pH 8.0 (Fig. 5). However, absorbance at 645–646 nm for R92A and R92L mutants was ~40% that of heme-WT, indicating that both mutants are less active than the wild-type enzyme. Absorption at 648 nm of verdoheme for the R92H and R92K mutants decreased with time, suggesting that verdoheme generated by the mutants was unstable to further oxidation. The k_{verdo} values at pH 6.0 were also obtained (Fig. 7, insets). Those for heme-R92A, heme-R92L, heme-R92H and heme-R92K mutants were 4.3 ± 0.5, 5.5 ± 0.4, 6.0 ± 0.2 and 5.3 ± 0.1 min^{-1}, respectively, which were approximately 5-fold smaller than that of heme-WT HutZ (23.3 ± 0.1 min^{-1}) in spite of almost similar amounts of the high-spin species, but close to those of for heme-R92A (3.5 ± 0.6 min^{-1}; Table 1), heme-R92L (2.7 ± 0.5 min^{-1}) and heme-R92H (3.2 ± 0.4 min^{-1}) mutants at pH 8.0. These results suggest that heme-Arg92 mutants are less active to verdoheme formation than heme-WT HutZ.

3.5. Reduction of heme-HutZ

The initial step of heme degradation by ascorbic acid is reduction of ferric heme (Supplemental Fig. S2) [33]. To clarify the reason for the lower heme degradation activity of Arg92 mutants, we measured the reduction rate (k_{red}) of the HutZ-bound heme. Since it was difficult to obtain the accurate reduction rates of heme in the case of HutZ owing to successive heme degradation and/or re-oxidation caused by contaminated molecular oxygen,

even under an anaerobic conditions, we measured the reduction rate in the presence of CO to irreversibly trap the generated ferrous heme as a CO-bound form [16]. The absorption spectral changes after addition of 1 mM ascorbic acid to ferric heme-HutZ are presented in Supplemental Fig. S3. Upon reduction, the Soret band at 407–408 nm underwent a red shift to 418 nm, the same position as the Soret band of the CO-bound form. The time-course of absorbance at 418 nm was fit to a single exponential or double exponential equation, generating k_{red} values for the heme-R92A, heme-R92L, heme-R92H and heme-R92K mutants of 18.0 ± 1.4/3.1 ± 0.2, 4.0 ± 0.6, 10.0 ± 1.0/2.5 ± 0.5 and 6.6 ± 1.3 h^{-1}, respectively, at pH 8.0 (Table 1), which were ~2–8-fold larger than that of heme-WT at pH 6.0 (2.4 ± 0.1 h^{-1}) [16]. In addition to the results of plots of $\nu_{Fe\text{-}CO}$ and $\nu_{C\text{-}O}$ (Fig. 3E), the k_{red} values for the heme-Arg92 mutants also supported the decrease in electron donation from the proximal histidine by removal of arginine at position 92.

3.6. Cyanide binding to heme-Arg92 mutants

To establish the effect of mutations of Arg92 on ligand binding to heme, cyanide (CN) binding kinetics of the heme-Arg92 mutants was investigated. The cyanide ion is generally used as a probe for assessing the accessibility of ligands to heme iron. Using a stopped-flow apparatus, the rate of CN binding was obtained. A typical time trace for the reaction of heme-WT HutZ with CN at 412 nm is shown in Supplemental Fig. S4A. Under conditions of excess cyanide, the pseudo-first-order rate constant value, k_{obs}, was obtained from a single-exponential fit (Supplemental Fig. S4A). The obtained k_{obs} value linearly increased with CN concentration (Supplemental Fig. S4B). The slope yielded the second-order rate constant ($k_{on,CN}$). The value for heme-WT HutZ was 0.88 ± 0.01 $mM^{-1}s^{-1}$ [43], while those for heme-R92A, heme-R92L, heme-R92H, and heme-R92K mutants were 0.52 ± 0.01, 0.83 ± 0.03, 0.87 ± 0.01, and 1.47 ± 0.03 $mM^{-1}s^{-1}$, respectively (Table 1), indicating that replacement of Arg92 does not hamper the ligand binding property of HutZ.

3.7. Fluorescence spectra of heme-Arg92 mutants

A recent investigation by our group showed that the relative positioning of two protomers is important in determining the heme degradation activity of HutZ [16]. Accordingly, we measured fluorescence spectra of the Arg92 mutants in this study to determine quaternary structural changes. HutZ contains tryptophan at position 109, which is predicted to be located ~21 Å from heme based on the crystal structure of HugZ from *H. pylori* (Supplemental Fig. S5) [29]. Quaternary structural changes were estimated by energy transfer efficiency from the tryptophan residue to heme, which is dependent on the distance between heme and tryptophan as described in Equation 1.

Fluorescence spectra of the apo and heme-bound R92A mutants are shown in Fig. 8A. The fluorescence intensity of the heme-R92A mutant was ~40% of the apo form, which was significantly larger than that of WT protein (3–5%) [16]. According to Equation 1, the distance was calculated as 21–26 Å (Fig. 8E), which was markedly larger than that of WT enzyme (16–18 Å) [16]. The same behavior was observed for the R92L and R92K mutants (Fig. 8B, D). In contrast, the distance of R92H mutant at pH 6–7 was relatively closer than that of WT HutZ, whereas that at pH >8 was much longer than that of WT HutZ, indicating that arginine at position 92 is necessary for HutZ to form an appropriate quaternary structure.

As described above, the distance was estimated as 16–17 Å for heme-WT HutZ [16] and mutation of Arg92 led to an increase in distance up to ~26 Å (Table 1). Asp132 is presumed to form a hydrogen bond with the heme axial ligand His170 from another protomer [20]. We additionally examined changes in the distance induced by disruption of the proximal hydrogen bond by substituting Asp132 for leucine. Fluorescence of Trp109 in the heme-D132L mutant was significantly increased (Supplemental Fig. S6). The distance between heme and Trp109 was estimated as ~26 Å, clearly indicating that mutation of Asp132 leads to elongation of distance. Our results collectively suggest that the proximal hydrogen bond contributes to subunit-subunit interactions.

4. Discussion

4.1. The spin state of heme is not a regulatory factor for the heme degradation reaction of HutZ

As reported by our group, HutZ from *V. cholerae* displays heme degradation ability with pH dependence [15,16]. The spin state of heme is also pH-dependent and HutZ is active when heme is in the high-spin state [15,16]. The spin state of heme is considered to reflect the protonation (Fe^{3+}-H_2O) or deprotonation (Fe^{3+}-OH^-) state of the iron-bound water molecule [44]. This acid-base transition is generally correlated with changes in the protonation status of a residue near the heme-bound water ligand [45]. Since the crystal structure of HugZ suggests that Arg92 of HutZ interacts with the heme-bound water molecule (Fig. 1), we replaced Arg92 with alanine or leucine to disrupt interactions or histidine or lysine to preserve the ability of the residue at this position to interact with the heme-bound ligand. Although the side-chains of histidine and lysine are shorter than that of arginine, these residues may form a hydrogen bond with the iron-bound water molecule. Mutation of Arg92 led to blue shift of the Soret maximum (Fig. 2), indicating an increase in high-spin heme at pH 8.0 owing to lower electrostatic interactions with the Fe^{3+}-OH^- species. However, ascorbic acid-assisted heme degradation activity of all Arg92 mutants was extremely low (Fig. 4). Thus, we conclude that the high-spin content of heme-HutZ is not the only factor to determine ascorbic acid-assisted heme degradation activity.

4.2. Electron donation from proximal histidine is a possible regulatory factor in the heme degradation reaction of HutZ

Under neutral or alkaline conditions, the proximal hydrogen bond between His170 and Asp132 enhances electron donation from the proximal histidine, leading to a slow reduction rate of heme iron owing to stabilization of the ferric heme [20], as observed for most peroxidases [30].

Replacement of distal Arg92 with alanine influenced the electrostatic nature of proximal histidine. The reduction rates of heme (k_{red}) in heme-Arg92 mutants were increased 4-9 fold (Table 1), suggesting that disruption of electrostatic interactions at the heme distal site alters the strength of the proximal hydrogen bond between His170 and Asp132. The correlation between $\nu_{Fe\text{-}CO}$ and $\nu_{C\text{-}O}$ in heme-Arg92 mutants supported the conclusion that electron donation from proximal histidine is diminished by removal of the distal hydrogen bond owing to mutation of Arg92 (Fig. 3E). The redox potential (E_m) for the heme-R92A mutant was shifted to a value ~30 mV higher than that of heme-WT HutZ (Supplemental Fig. S7) and closer to that of HO-1 than other peroxidases [21,46,47]. However, mutation of Arg92 did not lead to enhancement of activity (Fig. 4).

The same trend was observed for Asp132 mutants. Replacement of Asp132 with alanine or leucine reduced electron donation from His170 while heme degradation activity was almost completely lost [20]. Upon substitution of Asp132 with glutamic acid, a hydrogen bond between Glu132 and His170 was formed and enzymatic activity retained. Mutational analysis of Arg92 coincided with data on Asp132 mutants. While the mutation led to lower enhancement of electron donation from the proximal histidine, enzymatic activity remained low. Accordingly, we conclude that electron donation from His170 is a potential determinant of the heme degradation reaction of HutZ and altered by interactions of Arg92 with the iron-bound ligand.

4.3. Inactivation mechanism of heme-Arg92 mutants

The inactivation of Arg92 mutants can be accounted for slow protonation of the reduced oxyferrous heme, as discussed below. The reaction mechanism of heme degradation by HutZ was previously determined [35] (Supplemental Fig. S2). Under our experimental conditions whereby heme was already reconstituted with the enzyme, the first step of heme degradation was reduction of heme iron (step A, Supplemental Fig. S2). The k_{red} of heme-Arg92 mutants was increased 4-9 fold, compared with that of heme-WT HutZ (Table 1). The mutants reacted

with H_2O_2 to form verdoheme at the almost same rate as heme-WT HutZ (Fig. 5), indicating that once the hydroperoxy heme (Fe^{3+}–OOH) is formed, the heme degradation reaction proceeds in these mutants (steps D–E, Supplemental Fig. S2). Ligand binding rates (k_{CN}) of the Arg92 mutants were almost identical to that of heme-WT HutZ (Table 1), suggesting that O_2 binding to ferrous heme is not significantly affected by the mutation (step B, Supplemental Fig. S2). Although the kinetic data for reduction of oxyferrous heme are not available (step C, Supplemental Fig. S2), this step should not be slowed down by the Arg92 mutation, considering that k_{red} of the mutants was larger than that of heme-WT HutZ (Table 1). Altogether, our data indicate that protonation of the reduced oxyferrous heme (step C, Supplemental Fig. S2) is a putative bottleneck of the catalytic reaction of the Arg92 mutants, as observed from inactivation of HutZ in the presence of iron chelators [43].

There are at least three non-mutually exclusive explanations for the slow protonation of the reduced oxyferrous heme. A possible explanation for slow protonation of reduced oxyferrous heme of the Arg92 mutants is difference in pK_a values of the residue at position 92. The pK_a values of the side-chains of histidine, lysine and arginine were determined as 7.59, 9.74 and 10.8 [48] while those of the equilibrium between Fe^{3+}-H_2O and Fe^{3+}-OH^- for heme-R92H, heme-R92K mutants and WT HutZ were 8.1, 7.9 and 6.0 [15], respectively (Supplemental Fig. S1). The largest pK_a value was obtained for arginine while that of WT HutZ (Arg92) was the smallest. In a hydrophobic environment, such as a protein interior, the pK_a value tends to shift to neutral pH, probably owing to a local decrease in the dielectric constant [49]. Therefore, it is possible that only Arg92 is able to act as a proton donor to reduce oxyferrous heme whereas the side chains of His92 and Lys92 cannot act as proton donors.

There is a possibility that the introduced side chain at position 92 is not located at appropriate position for proton transfer even though the pK_a of histidine or lysine are suitable for proton transfer. However, the frequencies of $\nu_{Fe\text{-}CO}$ for the heme-R92H and heme-R92K mutants were close to that of heme-WT HutZ, indicating that both histidine and arginine in

the mutants are located close to the heme ligand.

A close examination of the structure of HugZ around the heme revealed a cluster of water molecules between Arg92 and Thr27 in HutZ (Fig. 9). Previously, we suggested that this cluster is involved in proton transfer to Fe^{3+}–OO^{-} (step C, Supplemental Fig. S2) [43]. Upon replacement of Thr27 with valine, ascorbic acid-assisted heme degradation reaction proceeded very slowly and the yield of iron release from heme decreased from 86 ± 7 to 61 ± 5%. In contrast, the serine mutant of Thr27 retained the rate and amount of iron release (83 ± 3%), indicating that water molecules form hydrogen bonds with Thr27 and function as a proton source. The importance of a water cluster as a proton source has also been demonstrated in HO [17,50]. These results suggest that mutation of Arg92 results in perturbation of localization of water molecules, making it difficult for Fe^{3+}–OO^{-} species to accept protons from the cluster and leading to loss of activity.

4.4. Regulatory Mechanisms of Heme Degradation by HutZ

Recently, we showed that orientation changes at the dimer interface present a key factor in controlling heme degradation activity [16]. Thus, it is feasible that quaternary structural changes occurring in the Arg92 mutants inactivate ascorbic acid-assisted heme degradation. To confirm this finding, we assessed fluorescence spectra of heme-HutZ. Structural changes at the dimer interface were estimated by measuring the distance between heme and Trp109 present in different protomers containing the axial heme ligand. The distance was calculated using Equation 1, since the decrease in fluorescence of Trp109 caused by energy transfer to heme depends on distance. Lowering the pH from 8.0 to 6.0 results in the increase in the distance by <2 Å, which leads to enhancement of heme degradation activity owing to weakening the hydrogen bond between His170 and Asp132 to decrease electron donation from His170 [16]. Upon replacement of Ala31 located at the dimer interface with valine, the distance expanded from 16–17 Å for WT HutZ to 24–27 Å [16]. Since the A31V mutant was

inactive in ascorbic acid-mediated heme degradation, we propose that the elongated dimer orientation of the heme-A31V mutant is not appropriate for function as a heme degradation enzyme. In the case of heme-Arg92 mutants, the distance between heme and Trp109 is greater than that of WT HutZ (Fig. 8), similar to that observed for the heme-A31V mutant [16]. Thus, modulation of the dimer interface in the Arg92 mutants would lead to loss of heme degradation activity.

We have already found that this distance is determined by some amino acid residues and related to enzymatic activity. When Asp132 was replaced with leucine (D132L), the distance between heme and Trp109 was greatly increased (Supplemental Fig. S6), similar to that for the R92A and R92L mutants (Fig. 8).

Changes of the subunit-subunit interactions also occurred in the His63 mutant [19]. His63 is presumed to be located close to heme and in the same subunit containing Asp132 but a different subunit from His170 and Arg92 (Supplemental Fig. S8). The distance between heme and Trp109 for the H63L mutant was significantly increased to 22–32 Å [19]. Accordingly, we propose that although Arg92 is present in the distal heme pocket, its mutation influences subunit-subunit interactions through Asp132 and His63 located within a different subunit, leading to increased distance between heme and Trp109 in the heme proximal site.

On the basis of these results, we propose the following scenario: Arg92 interacts with heme-bound OH^- at neutral pH under which HutZ is inactive for ascorbic acid-assisted heme degradation (Fig. 10). When H^+ binds to Fe^{3+}-OH^- to form high-spin heme (Fe-H_2O), the interaction between Arg92 and heme ligand is weakened (Fig. 10, **1**). This change is transmitted to the dimer interface including Ala31 (Fig. 10, **2**), which leads to modulation of subunit-subunit interactions (Fig. 10, **3**). This information is further transferred to Asp132 *via* His63 (Fig. 10, **4, 5**). As a result, the distance between subunits is elongated, weakening the interactions between Asp132 and His170 (Fig. 10, **6**). Owing to this structural domino effect

from Arg92 to Asp132, electron donation from His170 to heme iron is decreased, leading to an increased rate of heme reduction to promote heme degradation.

5. Conclusion

In summary, disruption of electrostatic interactions of Arg92 with the heme-bound water molecule led to loss of enzymatic activity of HutZ (Figs. 4, 6) caused by cleavage of the hydrogen bond between the heme axial ligand His170 and Asp132 [20]. In the absence of arginine at position 92, the distance between heme and Trp109 was significantly increased, indicating a change in the orientation of protomers. Such changes of subunit-subunit interactions influence the imidazolate character of the proximal histidine (Fig. 8) and propensity of heme reduction (Table 1). The findings that verdoheme, a characteristic intermediate of the heme degradation process, was formed during the reaction of Arg92 mutants with H_2O_2 (Figs. 5, 7) and kinetic parameters (k_{red}, k_{CN}) were favorably altered to promote heme degradation by the mutants suggest that H^+ transfer to the reduced oxyheme heme cannot proceed upon removal of Arg92, as observed for Ala31 mutants [16]. Because hHOs are monomeric and the common proximal hydrogen bond in most peroxidases is present within the same subunit, the intersubunit hydrogen bond between His170 and Asp132 is a characteristic feature of HutZ. Furthermore, in most heme enzymes, arginine is used for stabilization of reaction intermediates but not acid-alkaline catalysis [51,52]. However, the pK_a of the side-chain of arginine would be suitable for acid-base catalyst activity in the heme degradation reaction of HutZ. Iron is an essential element for bacterial survival but excessive quantities are harmful due to generation of free radicals and consequent oxidative stress, highlighting the need for strict regulation of iron uptake. The activation mechanism of HutZ uncovered in this study may play a critical role in iron homeostasis in *V. cholerae*.

Abbreviation List

HO heme oxygenase

hHO human heme oxygenase
WT wild-type.

Acknowledgements

This study was supported in part by Grants-in-Aid for Scientific Research (18J10820 to N.D., 16K05835 to T.U., and 19H05769 to K.I.) from the Ministry of Culture, Education, Sports, Science, and Technology (MEXT) of Japan.

Appendix A. Supplementary data

Supplementary data to this article can be found online at

Competing Interests

The authors declare that there are no competing interests associated with the manuscript.

References

[1] L.L. Anzaldi, E.P. Skaar, Overcoming the heme paradox: Heme toxicity and tolerance in bacterial pathogens, Infect. Immun. 78 (2010) 4977–4989. doi:10.1128/IAI.00613-10.

[2] C.A. Genco, D.W. Dixon, Emerging strategies in microbial haem capture, Mol. Microbiol. 39 (2001) 1–11. doi:10.1046/j.1365-2958.2001.02231.x.

[3] U.A. Ochsner, Z. Johnson, M.L. Vasil, Genetics and regulation of two distinct haem-uptake systems, phu and has, in Pseudomonas aeruginosa, Microbiology. 146 (2000) 185–198. doi:doi:10.1099/00221287-146-1-185.

[4] J.A. Stoebner, S.M. Payne, Iron-regulated hemolysin production and utilization of heme and hemoglobin by Vibrio cholerae., Infect. Immun. 56 (1988) 2891–2895. http://www.pubmedcentral.nih.gov/articlerender.fcgi?artid=259667&tool=pmcentrez&rendertype=abstract.

[5] C. Wandersman, I. Stojiljkovic, Bacterial heme sources: the role of heme, hemoprotein receptors and hemophores, Curr. Opin. Microbiol. 3 (2000) 215–220. doi:10.1016/S1369-5274(00)00078-3.

[6] A. Wilks, K.A. Burkhard, Heme and virulence: how bacterial pathogens regulate, transport and utilize heme., Nat. Prod. Rep. 24 (2007) 511–522. doi:10.1039/b604193k.

[7] J.F. Heidelberg, J.A. Eisen, W.C. Nelson, R. a Clayton, M.L. Gwinn, R.J. Dodson, D.H.

Haft, E.K. Hickey, J.D. Peterson, L. Umayam, S.R. Gill, K.E. Nelson, T.D. Read, H. Tettelin, D. Richardson, M.D. Ermolaeva, J. Vamathevan, S. Bass, H. Qin, I. Dragoi, P. Sellers, L. McDonald, T. Utterback, R.D. Fleishmann, W.C. Nierman, O. White, S.L. Salzberg, H.O. Smith, R.R. Colwell, J.J. Mekalanos, J.C. Venter, C.M. Fraser, DNA sequence of both chromosomes of the cholera pathogen Vibrio cholerae., Nature. 406 (2000) 477–483. doi:10.1038/35020000.

[8] E.E. Wyckoff, M. Schmitt, A. Wilks, S.M. Payne, HutZ is required for efficient heme utilization in Vibrio cholerae, J. Bacteriol. 186 (2004) 4142–4151. doi:10.1128/JB.186.13.4142.

[9] E.E. Wyckoff, A.R. Mey, S.M. Payne, Iron acquisition in Vibrio cholerae., Biometals. 20 (2007) 405–416. doi:10.1007/s10534-006-9073-4.

[10] D.P. Henderson, S.M. Payne, Characterization of the Vibrio cholerae outer membrane heme transport protein HutA: sequence of the gene, regulation of expression, and homology to the family of TonB-dependent proteins., J. Bacteriol. 176 (1994) 3269–3277. http://jb.asm.org/cgi/content/abstract/176/11/3269.

[11] D.A. Occhino, E.E. Wyckoff, D.P. Henderson, T.J. Wrona, S.M. Payne, Vibrio cholerae iron transport: haem transport genes are linked to one of two sets of tonB, exbB, exbD genes., Mol. Microbiol. 29 (1998) 1493–1507. http://www.ncbi.nlm.nih.gov/pubmed/9781885 (accessed August 9, 2017).

[12] A.R. Mey, S.M. Payne, Haem utilization in Vibrio cholerae involves multiple TonB-dependent haem receptors., Mol. Microbiol. 42 (2001) 835–849. http://www.ncbi.nlm.nih.gov/pubmed/11722746 (accessed November 9, 2016).

[13] T. Uchida, T. Funamizu, M. Ogura, K. Ishimori, Heme iron coordination structure of heme transport protein HutB from Vibrio cholerae, Bull. Chem. Soc. Jpn. 90 (2017) 924–930. doi:10.1246/bcsj.20170104.

[14] Y. Sekine, T. Tanzawa, Y. Tanaka, K. Ishimori, T. Uchida, Cytoplasmic heme-binding protein (HutX) from Vibrio cholerae is an intracellular heme transport protein for the heme-degrading enzyme, HutZ, Biochemistry. 55 (2016) 884–893. doi:10.1021/acs.biochem.5b01273.

[15] T. Uchida, Y. Sekine, T. Matsui, M. Ikeda-Saito, K. Ishimori, A heme degradation enzyme, HutZ, from Vibrio cholerae, Chem. Commun. 48 (2012) 6741–6743. doi:10.1039/c2cc31147j.

[16] T. Uchida, K. Ota, Y. Sekine, N. Dojun, K. Ishimori, Subunit-subunit interactions play a key role in the heme-degradation reaction of HutZ from Vibrio cholerae, Dalton Trans. 48 (2019) 3973–3983. doi:10.1039/C9DT00604D.

[17] H. Fujii, X. Zhang, T. Tomita, M. Ikeda-Saito, T. Yoshida, A role for highly conserved carboxylate, aspartate-140, in oxygen activation and heme degradation by heme oxygenase-1., J. Am. Chem. Soc. 123 (2001) 6475–6484. doi:10.1021/ja010490a.

[18] X. Liu, Q. Du, Z. Wang, D. Zhu, Y. Huang, N. Li, T. Wei, S. Xu, L. Gu, Crystal structure and Biochemical features of EfeB/YcdB from Escherichia coli O157: ASP235 plays divergent roles in different enzyme-catalyzed processes, J. Biol. Chem. 286 (2011) 14922–14931. doi:10.1074/jbc.M110.197780.

[19] T. Uchida, N. Dojun, Y. Sekine, K. Ishimori, Role of His63 in HutZ from Vibrio cholerae in the heme degradation reaction and heme binding, Dalton Trans. 48 (2019) 5408–5416. doi:10.1039/C9DT00926D.

[20] T. Uchida, N. Dojun, Y. Sekine, K. Ishimori, Heme proximal hydrogen bonding between His170 and Asp132 plays an essential role in the heme degradation reaction of HutZ from Vibrio cholerae, Biochemistry. 56 (2017) 2723–2734. doi:10.1021/acs.biochem.7b00152.

[21] D.B. Goodin, D.E. McRee, The Asp-His-Fe triad of cytochrome c peroxidase controls the reduction potential, electronic structure, and coupling of the tryptophan free radical to the heme., Biochemistry. 32 (1993) 3313–3324. http://eutils.ncbi.nlm.nih.gov/entrez/eutils/elink.fcgi?dbfrom=pubmed&id=8384877&retmode=ref&cmd=prlinks%5Cnpapers3://publication/uuid/6C016A35-7FB8-4E94-9E84-F0AAA761AAC4.

[22] T.L. Poulos, Peroxidases, Curr. Opin. Biotechnol. 4 (1993) 484–489. doi:10.1016/0958-1669(93)90016-P.

[23] M. Gajhede, D.J. Schuller, A. Henriksen, A.T. Smith, T.L. Poulos, Crystal structure of horseradish peroxidase C at 2.15 Å resolution., Nat. Struct. Biol. 4 (1997) 1032–8. http://www.ncbi.nlm.nih.gov/pubmed/9406554 (accessed August 2, 2016).

[24] G.B. Ray, X.Y. Li, J.A. Ibers, J.L. Sessler, T.G. Spiro, How far can proteins bend the FeCO unit - Distal polar and steric effects in heme-proteins and models, J. Am. Chem. Soc. 116 (1994) 162–176. doi:10.1021/ja00080a019.

[25] B.A. Springer, S.G. Sligar, J.S. Olson, G. Phillips, Jr., Mechanisms of ligand recognition in myoglobin, Chem. Rev. 94 (1994) 699–714. doi:10.1021/cr00027a007.

[26] G.N. Phillips, M.L. Teodoro, T. Li, B. Smith, J.S. Olson, Bound CO is a molecular probe of electrostatic potential in the distal pocket of myoglobin, J. Phys. Chem. B. 103 (1999) 8817–8819. doi:10.1021/jp9918205.

[27] T.G. Spiro, I.H. Wasbotten, CO as a vibrational probe of heme protein active sites, J. Inorg. Biochem. 99 (2005) 34–44. doi:10.1016/j.jinorgbio.2004.09.026.

[28] S. Takahashi, J.L. Wang, D.L. Rousseau, K. Ishikawa, T. Yoshida, N. Takeuchi, M. Ikeda-Ssaito, Heme-heme oxygenase complex: Structure and properties of the catalytic site from resonance Raman scattering, Biochemistry. 33 (1994) 5531–5538. doi:10.1021/bi00184a023.

[29] Y. Hu, F. Jiang, Y. Guo, X. Shen, Y. Zhang, R. Zhang, G. Guo, X. Mao, Q. Zou, D.-C. Wang, Crystal structure of HugZ, a novel heme oxygenase from Helicobacter pylori., J. Biol. Chem. 286 (2011) 1537–1544. doi:10.1074/jbc.M110.172007.

[30] B.H. Dunford, Heme Peroxidases, Wiley-VCH, New York, 1999.

[31] D.J. Schuller, A. Wilks, P.R. Ortiz de Montellano, T.L. Poulos, Crystal structure of human heme oxygenase-1., Nat. Struct. Biol. 6 (1999) 860–867. doi:10.1038/12319.

[32] Y. Liu, L. Koenigs Lightning, H. Huang, P. Moënne-Loccoz, D.J. Schuller, T.L. Poulos, T.M. Loehr, P.R. Ortiz de Montellano, Replacement of the distal glycine 139 transforms human heme oxygenase-1 into a peroxidase., J. Biol. Chem. 275 (2000) 34501–34507. doi:10.1074/jbc.M004245200.

[33] T. Uchida, Y. Sekine, N. Dojun, A. Lewis-Ballester, I. Ishigami, T. Matsui, S.-R. Yeh, K. Ishimori, Reaction intermediates in the heme degradation reaction by HutZ from Vibrio cholerae, Dalt. Trans. 46 (2017) 8104–8109. doi:10.1039/C7DT01562C.

[34] R.M.C. Dawson, D.C. Elliot, W.H. Elliot, K.M. Jones, Data for Biochemical Research, Oxford University Press Inc., New York, 1995. https://global.oup.com/academic/product/data-for-biochemical-research-9780198552994?cc=jp&lang=en&.

[35] T. Uchida, N. Kobayashi, S. Muneta, K. Ishimori, The iron chaperone protein CyaY from Vibrio cholerae is a heme-binding protein, Biochemistry. 56 (2017) 2425–2434. doi:10.1021/acs.biochem.6b01304.

[36] P. Wu, L. Brand, Resonance energy transfer: methods and applications., Anal. Biochem. 218 (1994) 1–13. http://www.ncbi.nlm.nih.gov/pubmed/8053542 (accessed October 11, 2017).

[37] L.L. Stookey, Ferrozine–A new spectrophotometric reagent for iron, Anal. Chem. 42 (1970) 779–781. doi:10.1021/ac60289a016.

[38] S.W. Englander, D.B. Calhoun, J.J. Englander, Biochemistry without oxygen., Anal. Biochem. 161 (1987) 300–306. doi:10.1016/0003-2697(87)90454-4.

[39] X. Liu, J. Gong, T. Wei, Z. Wang, Q. Du, D. Zhu, Y. Huang, S. Xu, L. Gu, Crystal structure of HutZ, a heme storage protein from Vibrio cholerae: A structural mismatch observed in the region of high sequence conservation, BMC Struct. Biol. 12 (2012) 23. doi:10.1186/1472-6807-12-23.

[40] S. Takahashi, J. Wang, D.L. Rousseau, K. Ishikawa, T. Yoshida, J.R. Host, M. Ikeda-Saito, Heme-heme oxygenase complex. Structure of the catalytic site and its implication for oxygen activation., J. Biol. Chem. 269 (1994) 1010–1014. http://www.ncbi.nlm.nih.gov/pubmed/8288555 (accessed July 25, 2016).

[41] T.G. Spiro, X.Y. Li, Resonance Raman spectroscopy of metalloporphyrins, in: T.G. Spiro (Ed.), Biol. Appl. Raman Spectrosc., III, John Wiley and Sons, New York, 1988: pp. 1–37.

[42] T. Kitagawa, Heme protein structure and the iron-histidine stretching mode, in: T.G. Spiro (Ed.), Biol. Appl. Raman Spectrosc., III, John Wiley & Sons, New York, 1988: pp. 97–131.

[43] N. Dojun, Y. Sekine, K. Ishimori, T. Uchida, Iron chelators inhibit the heme-degradation reaction by HutZ from Vibrio cholerae, Dalt. Trans. 46 (2017) 5147–5150. doi:10.1039/C7DT00121E.

[44] E. Antonini, M. Brunori, Hemoglobin and myoglobin in their reactions with ligands, Elsevier/North-Holland Biomedical Press, Amsterdam, 1971.

[45] M. Ikeda-Saito, H. Hori, L.A. Andersson, R.C. Prince, I.J. Pickering, G.N. George, C.R. Sanders, R.S. Lutz, E.J. McKelvey, R. Mattera, Coordination structure of the ferric heme iron in engineered distal histidine myoglobin mutants., J. Biol. Chem. 267 (1992) 22843–22852. http://www.ncbi.nlm.nih.gov/pubmed/1429633 (accessed July 31, 2017).

[46] S. Hashimoto, J. Teraoka, T. Inubushi, T. Yonetani, T. Kitagawa, Resonance Raman study on cytochrome c peroxidase and its intermediate, J. Biol. Chem. 261 (1986) 11110–11118.

[47] G. Smulevich, J.M. Mauro, L.A. Fishel, A.M. English, J. Kraut, T.G. Spiro, Heme pocket interactions in cytochrome, Biochemistry. 27 (1988) 5477–5485.

[48] D. Voet, J.G. Voet, Biochemistry, 4th ed., John Wiley & Sons, New York, 2011.

[49] Y. Xiao, M.S. Hutson, M. Belenky, J. Herzfeld, M.S. Braiman, Role of arginine-82 in fast proton release during the bacteriorhodopsin photocycle: A time-resolved FT-IR study of purple membranes containing 15N-labeled arginine, Biochemistry. 43 (2004) 12809–12818. doi:10.1021/bi049238g.

[50] T. Matsui, M. Furukawa, M. Unno, T. Tomita, M. Ikeda-Saito, Roles of distal Asp in heme oxygenase from Corynebacterium diphtheriae, HmuO: A water-driven oxygen activation mechanism., J. Biol. Chem. 280 (2005) 2981–2989. doi:10.1074/jbc.M410263200.

[51] J.N. Rodriguez-Lopez, A.T. Smith, R.N. Thorneley, Role of arginine 38 in horseradish

peroxidase. A critical residue for substrate binding and catalysis., J. Biol. Chem. 271 (1996) 4023–4030. http://www.ncbi.nlm.nih.gov/pubmed/8626735 (accessed November 21, 2017).

[52] R. Singh, J.C. Grigg, Z. Armstrong, M.E.P. Murphy, L.D. Eltis, Distal heme pocket residues of B-type dye-decolorizing peroxidase: arginine but not aspartate is essential for peroxidase activity., J. Biol. Chem. 287 (2012) 10623–10630. doi:10.1074/jbc.M111.332171.

[53] B.-S. Lou, J.K. Snyder, P. Marshall, J.-S. Wang, G. Wu, R.J. Kulmacz, A.-L. Tsai, J. Wang, Resonance Raman studies indicate a unique heme active site in prostaglandin H synthase., Biochemistry. 39 (2000) 12424–12434. http://www.ncbi.nlm.nih.gov/pubmed/11015223.

Table 1

Heme binding and reduction properties, and estimated distance between heme and Trp109 of WT and Arg92 mutant HutZ.

	k_{verdo}	k_{red}		k_{CN}	r
	min^{-1}	h^{-1}		$mM^{-1}\ s^{-1}$	Å
WT	0.55 ± 0.09[a]	0.86 ± 0.08[a]		0.88 ± 0.01	16–18
WT		2.4 ± 0.1[b]		–	–
R92A	3.5 ± 0.6[a]	18.0 ± 1.4[a]	(56 ± 9%)	0.52 ± 0.01	21–25
		3.1 ± 0.2[a]	(44 ± 9%)		
R92L	2.7 ± 0.5[a]	4.0 ± 0.6[a]		0.83 ± 0.03	23–26
R92H	3.2 ± 0.4[a]	10.0 ± 1.0[a]	(53 ± 18%)	0.87 ± 0.01	19–24
		2.5 ± 0.5[a]	(47 ± 18%)		
R92K	0.70 ± 0.05[a]	6.6 ± 1.3[a]		1.47 ± 0.03	17–26

[a]Data were measured in 50 mM Tris-HCl and 150 mM NaCl (pH 8.0). [b]This datum was measured in 50 mM Na-Pi and 150 mM NaCl (pH 6.0).

Figure legends

Fig. 1. **Crystal structures of a HutZ homologous protein HugZ from *Helicobacter pylori*** (PDB ID code 3GAS).
The residue numbering is based on *V. cholerae* HutZ. Arg92 in HugZ forms a hydrogen bond with iron-bound azide through a water molecule.

Fig. 2. Absorption spectra of ferric heme-Arg92 HutZ mutants.
The protein concentration was 5 μM (on a per heme basis) in 50 mM Tris-HCl and 150 mM

NaCl (pH 8.0) (red line) and 50 mM sodium phosphate and 150 mM NaCl (pH 6.0) (blue line). Insets show heme binding curve generated from the difference absorbance of the Soret maximum by plotting ΔAbs *vs.* molar ratios of heme to protein: (A) heme-WT, (B) heme-R92A, (C) heme-R92L, (D) heme-R92H, and (E) heme-R92K.

Fig. 3. Resonance Raman spectra of heme-Arg92 HutZ mutants.
The protein concentration was 10 μM in 50 mM Tris-HCl and 150 mM NaCl (pH 8.0). The excitation wavelength for the ferric and CO-bound forms was 413.1 nm, and that for the ferrous form was 441.6 nm: (A) ferric form in the high-frequency region, (B) ferrous form in the low-frequency region, (C) CO-bound form in the low-frequency region, and (D) CO-bound form in the high-frequency region. (E) Correlation between frequencies of $\nu_{Fe\text{-}CO}$ and $\nu_{C\text{-}O}$ stretching modes. The two solid lines correspond to correlations for proximal imidazoles (●), proximal imidazolate (▲), and thiolate-ligated hemoproteins (◆). The data point for heme-HutZ is presented as an open circle. Data showing an inverse correlation between $\nu_{Fe\text{-}CO}$ ves $\nu_{C\text{-}O}$ and taken from refs [24,27,53]. The protein concentration was 10 μM in 50 mM Tris-HCl and 150 mM NaCl (pH 8.0).

Fig. 4. **Heme degradation reaction of the heme-Arg92 HutZ mutants with ascorbic acid (1.0 mM) in 50 mM Tris-HCl and 150 mM NaCl (pH 8.0).**
Spectra were recorded before the addition of ascorbic acid (black line) and at 4-min intervals for 60 min after the addition of ascorbic acid (red line). Green line showed the spectra after addition of ferrozine 60 min after initiation of the reaction: (A) heme-R92A, (B) heme-R92L, (C) heme-R92H, and (D) heme-R92K.

Fig. 5. **Heme degradation reaction of the heme-Arg92 HutZ mutants with H_2O_2 (0.2 mM) in 50 mM Tris-HCl and 150 mM NaCl (pH 8.0).**
Spectra were recorded before the addition of H_2O_2 and at 1-min intervals for 15 min after the addition of H_2O_2: (A) heme-R92A, (B) heme-R92L, (C) heme-R92H, and (D) heme-R92K. The insets show the time course of absorbance at 645–648 nm after the addition of H_2O_2 obtained by stopped-flow measurements.

Fig. 6. Heme degradation reaction of the heme-Arg92 HutZ mutants with ascorbic acid (1.0 mM) in 50 mM sodium phosphate and 150 mM NaCl (pH 6.0).
Spectra were recorded before the addition of ascorbic acid (black line) and at 4-min intervals for 60 min after the addition of ascorbic acid (red line). Green line showed the spectra after addition of ferrozine 60 min after initiation of the reaction: (A) heme-WT, (B) heme-R92A, (C) heme-R92L, (D) heme-R92H, and (E) heme-R92K.

Fig. 7. Heme degradation reaction of the heme-Arg92 HutZ mutants with H_2O_2 (0.2 mM) in 50 mM sodium phosphate and 150 mM NaCl (pH 6.0).
Spectra were recorded before the addition of H_2O_2 and at 1-min intervals for 15 min after the

addition of ascorbic acid: (A) heme-WT, (B) heme-R92A, (C) heme-R92L, (D) heme-R92H, and (E) heme-R92K. The insets show the time course of absorbance at 644 nm after the addition of H_2O_2 obtained by stopped-flow measurements.

Fig. 8. Fluorescence spectra of the ferric (A) R92A, (B) R92L, (C) R92H and (D) R92K mutant HutZ s in the absence (blue lines) and presence of heme (red lines) at pH 6.0–9.0.
Spectra were recorded with excitation at 295 nm. The sample concentration was 3 μM. (E) pH dependence of the distance between heme and Trp109 estimated by quenching of tryptophan fluorescence by energy transfer efficiency and the Förster distance using equation 2.

Fig. 9. Crystal structures of a HutZ homologous protein HugZ from *H. pylori* (PDB ID code 3GAS).
The residue numbering is based on *V. cholerae* HutZ. A cluster of water molecules is formed between Arg92 and Thr27.

Fig. 10. Proposed regulation mechanism of heme degradation by HutZ *via* subunit-subunit interactions.
The numbers show the sequence of events occurred during conversion from inactive to active forms of HutZ.

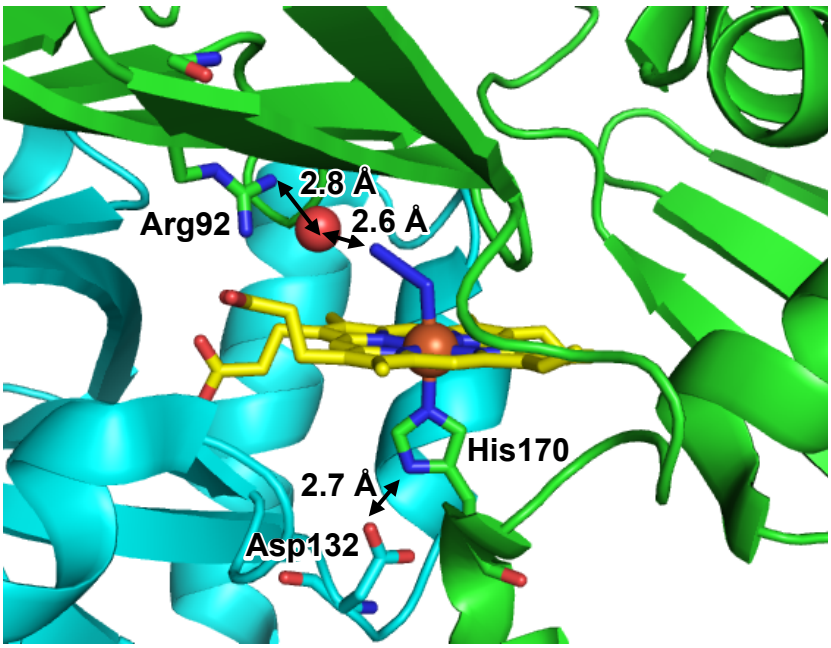

Fig. 1. **Crystal structures of a HutZ homologous protein HugZ from *Helicobacter pylori*** (PDB ID code 3GAS). The residue numbering is based on *V. cholerae* HutZ. Arg92 in HugZ forms a hydrogen bond with iron-bound azide through a water molecule.

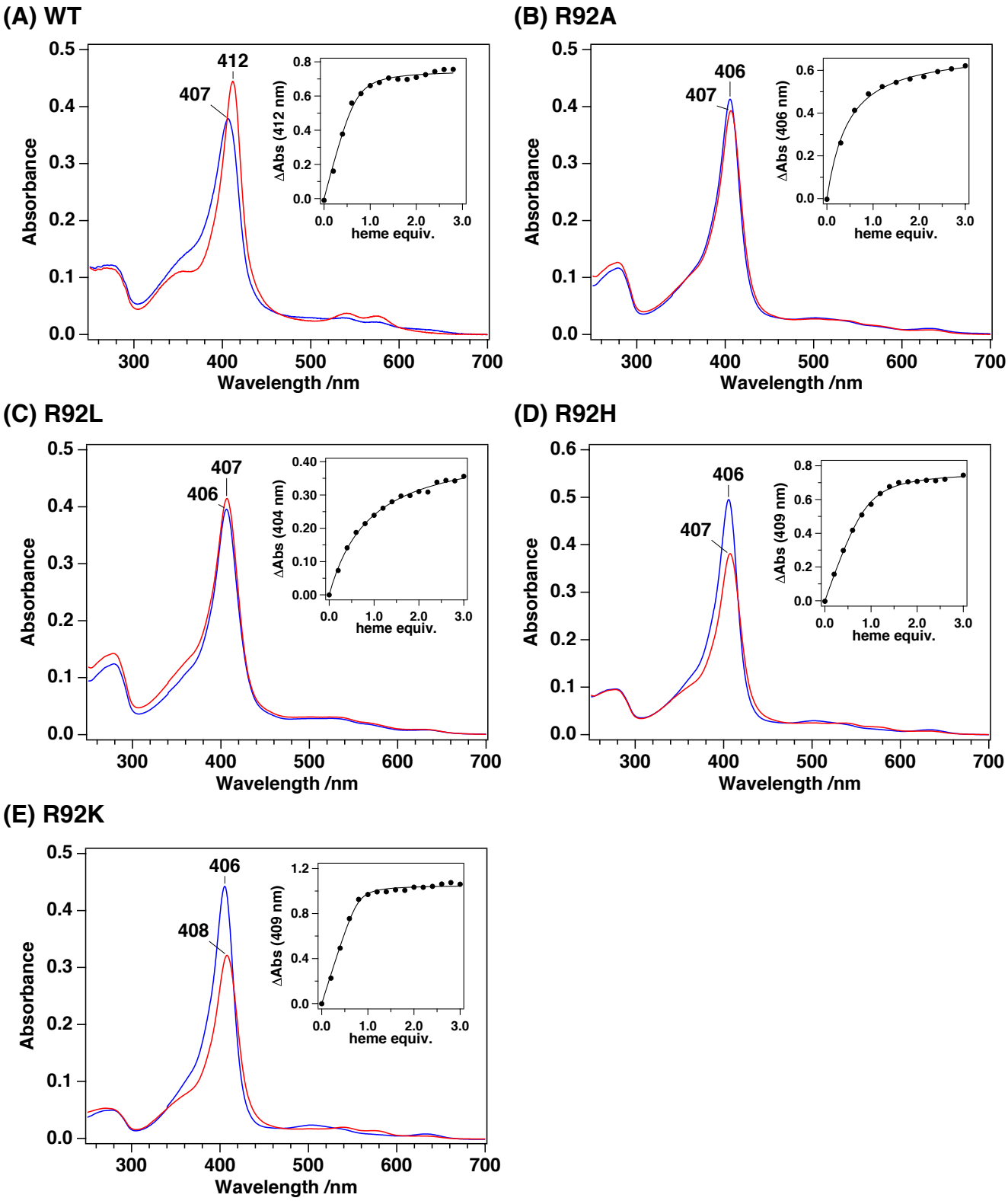

Fig. 2. Absorption spectra of ferric heme-Arg92 HutZ mutants. The protein concentration was 5 μM (on a per heme basis) in 50 mM Tris-HCl and 150 mM NaCl (pH 8.0) (red line) and 50 mM sodium phosphate and 150 mM NaCl (pH 6.0) (blue line). Insets show heme binding curve generated from the difference absorbance of the Soret maximum by plotting ΔAbs *vs.* molar ratios of heme to protein: (A) heme-WT, (B) heme-R92A, (C) heme-R92L, (D) heme-R92H, and (E) heme-R92K.

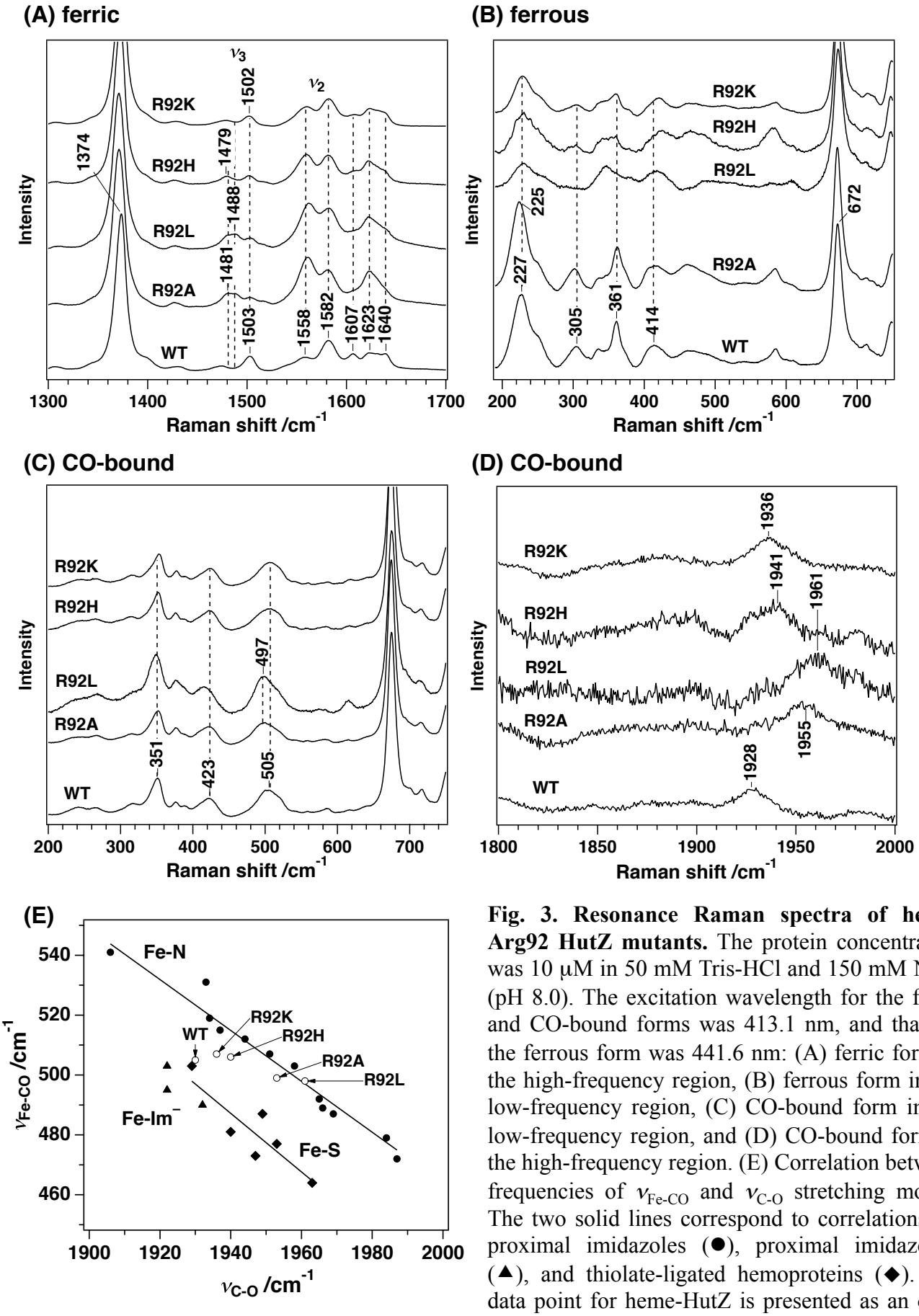

Fig. 3. Resonance Raman spectra of heme-Arg92 HutZ mutants. The protein concentration was 10 μM in 50 mM Tris-HCl and 150 mM NaCl (pH 8.0). The excitation wavelength for the ferric and CO-bound forms was 413.1 nm, and that for the ferrous form was 441.6 nm: (A) ferric form in the high-frequency region, (B) ferrous form in the low-frequency region, (C) CO-bound form in the low-frequency region, and (D) CO-bound form in the high-frequency region. (E) Correlation between frequencies of $\nu_{Fe\text{-}CO}$ and $\nu_{C\text{-}O}$ stretching modes. The two solid lines correspond to correlations for proximal imidazoles (●), proximal imidazolate (▲), and thiolate-ligated hemoproteins (◆). The data point for heme-HutZ is presented as an open circle. Data showing an inverse correlation between $\nu_{Fe\text{-}CO}$ ves $\nu_{C\text{-}O}$ and taken from refs [24,27,53]. The protein concentration was 10 μM in 50 mM Tris-HCl and 150 mM NaCl (pH 8.0).

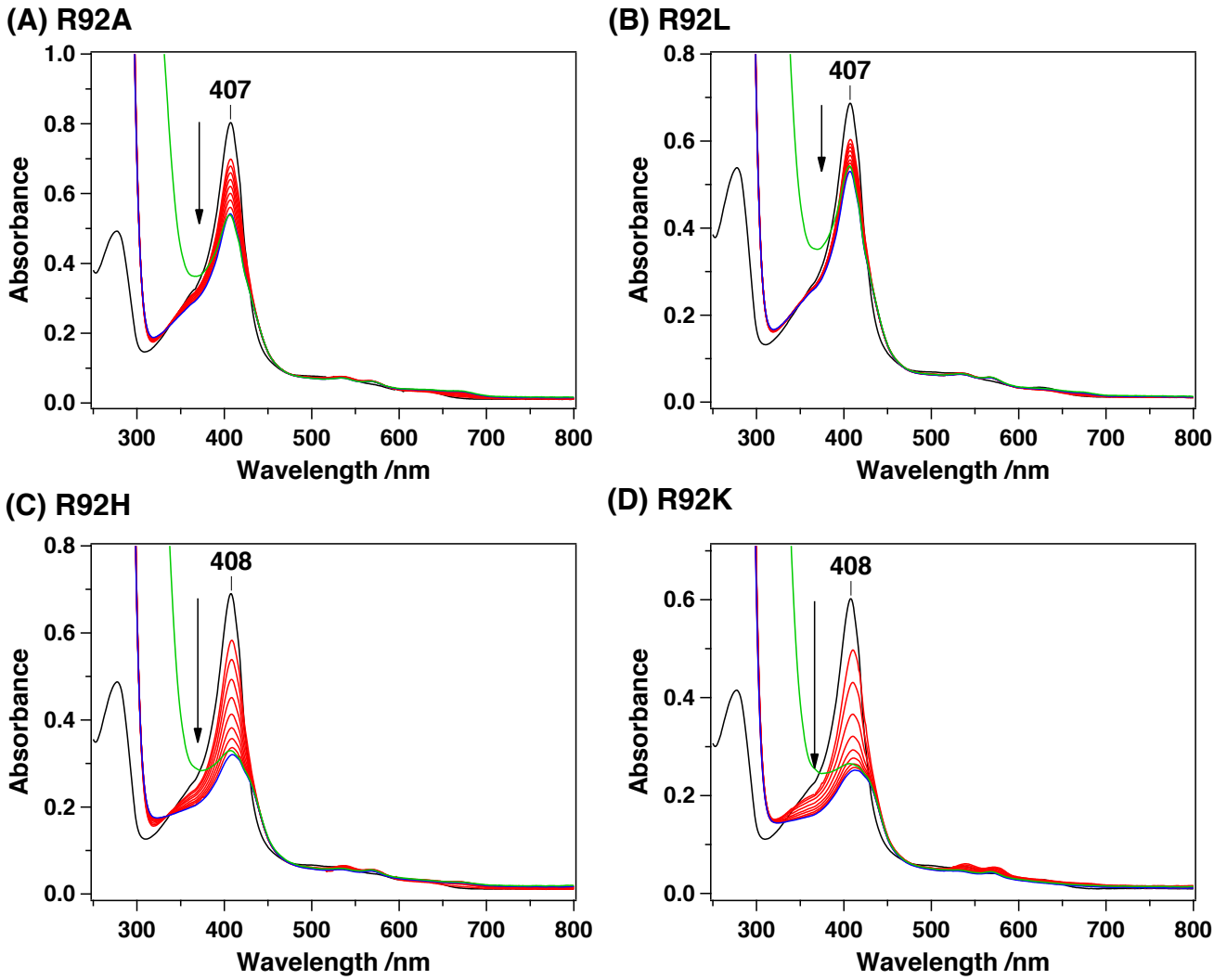

Fig. 4. Heme degradation reaction of the heme-Arg92 HutZ mutants with ascorbic acid (1.0 mM) in 50 mM Tris-HCl and 150 mM NaCl (pH 8.0). Spectra were recorded before the addition of ascorbic acid (black line) and at 4-min intervals for 60 min after the addition of ascorbic acid (red line). Green line showed the spectra after addition of ferrozine 60 min after initiation of the reaction: (A) heme-R92A, (B) heme-R92L, (C) heme-R92H, and (D) heme-R92K.

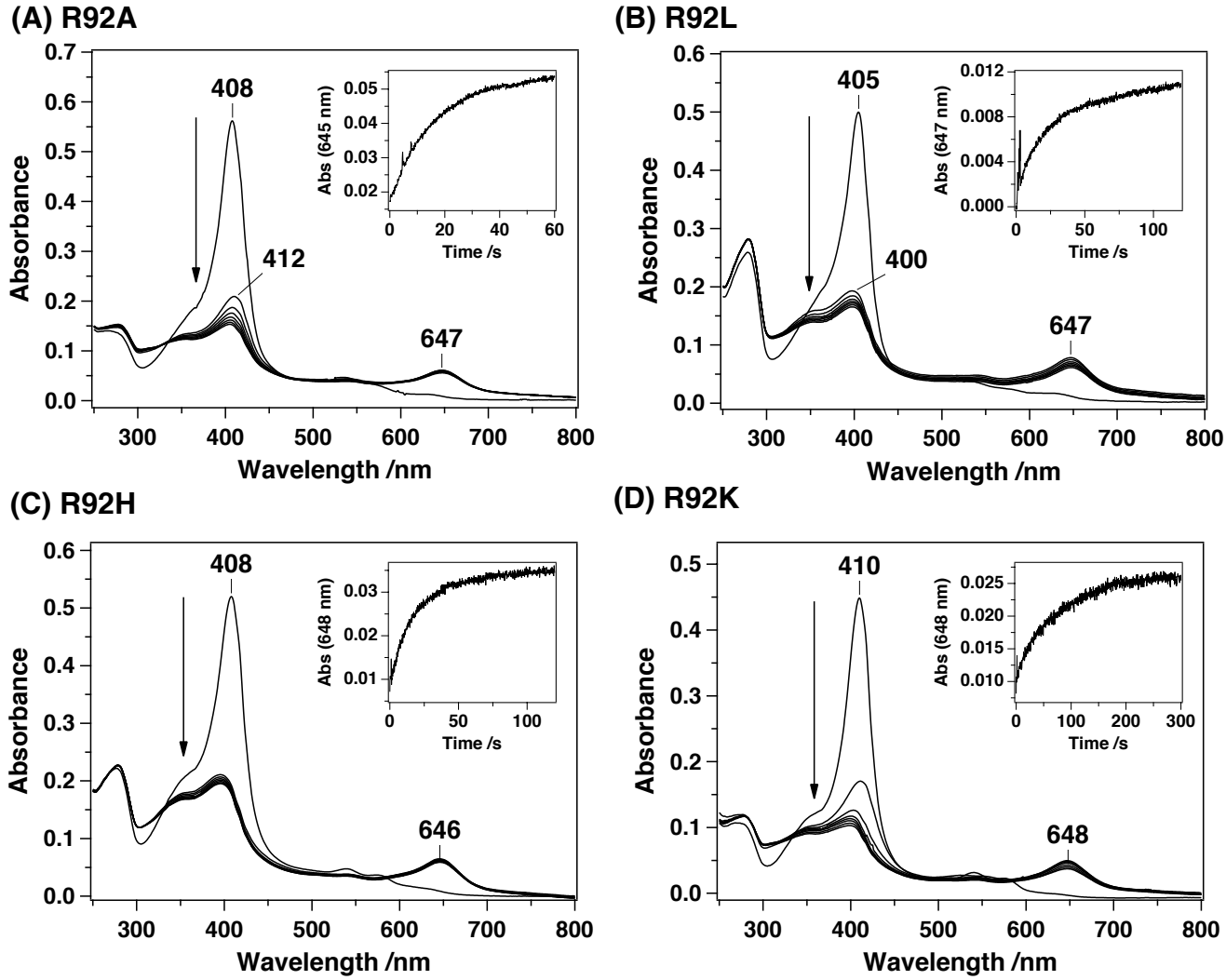

Fig. 5. **Heme degradation reaction of the heme-Arg92 HutZ mutants with H_2O_2 (0.2 mM) in 50 mM Tris-HCl and 150 mM NaCl (pH 8.0).** Spectra were recorded before the addition of H_2O_2 and at 1-min intervals for 15 min after the addition of H_2O_2: (A) heme-R92A, (B) heme-R92L, (C) heme-R92H, and (D) heme-R92K. The insets show the time course of absorbance at 645–648 nm after the addition of H_2O_2 obtained by stopped-flow measurements.

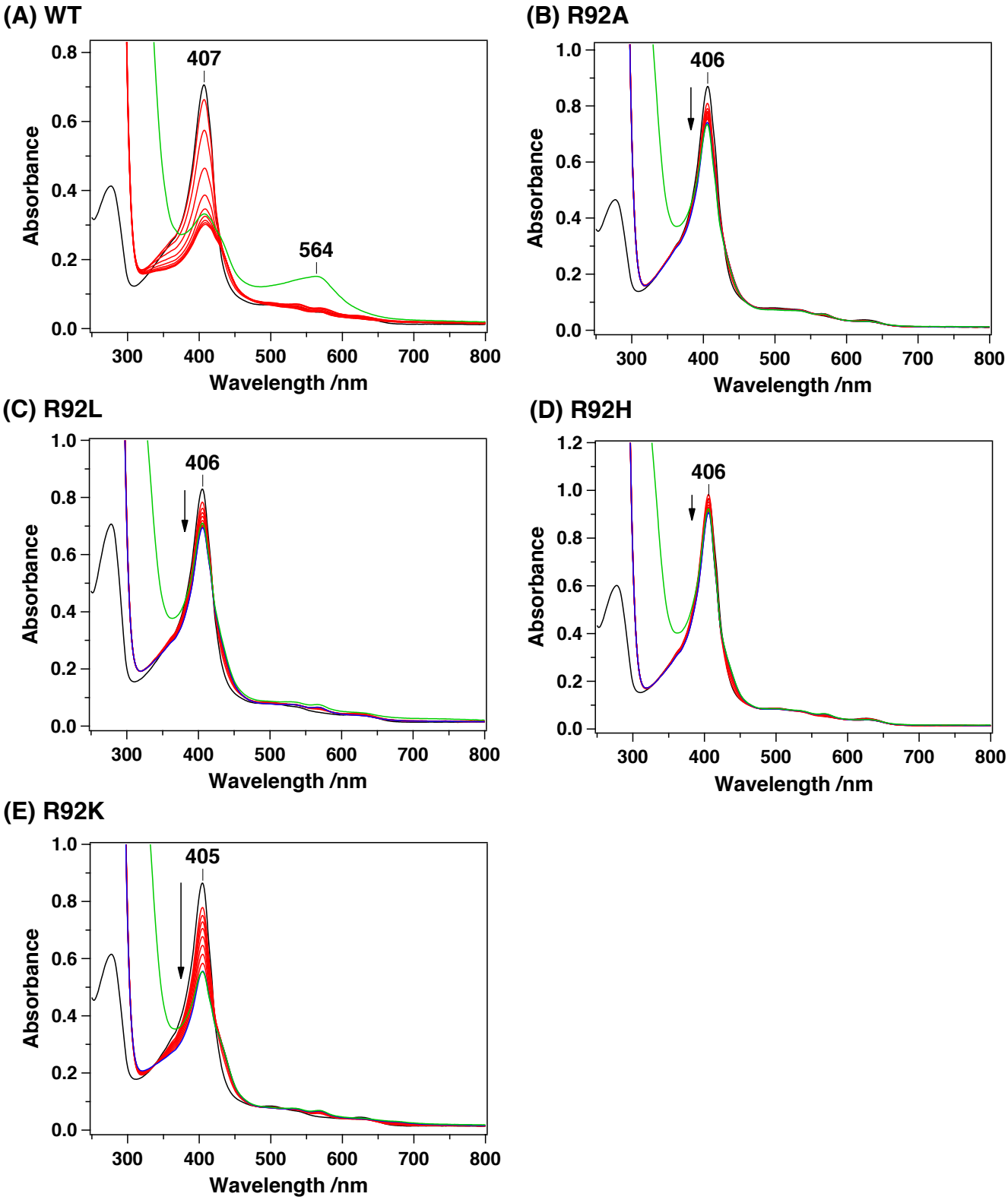

Fig. 6. Heme degradation reaction of the heme-Arg92 HutZ mutants with ascorbic acid (1.0 mM) in 50 mM sodium phosphate and 150 mM NaCl (pH 6.0). Spectra were recorded before the addition of ascorbic acid (black line) and at 4-min intervals for 60 min after the addition of ascorbic acid (red line). Green line showed the spectra after addition of ferrozine 60 min after initiation of the reaction: (A) heme-WT, (B) heme-R92A, (C) heme-R92L, (D) heme-R92H, and (E) heme-R92K.

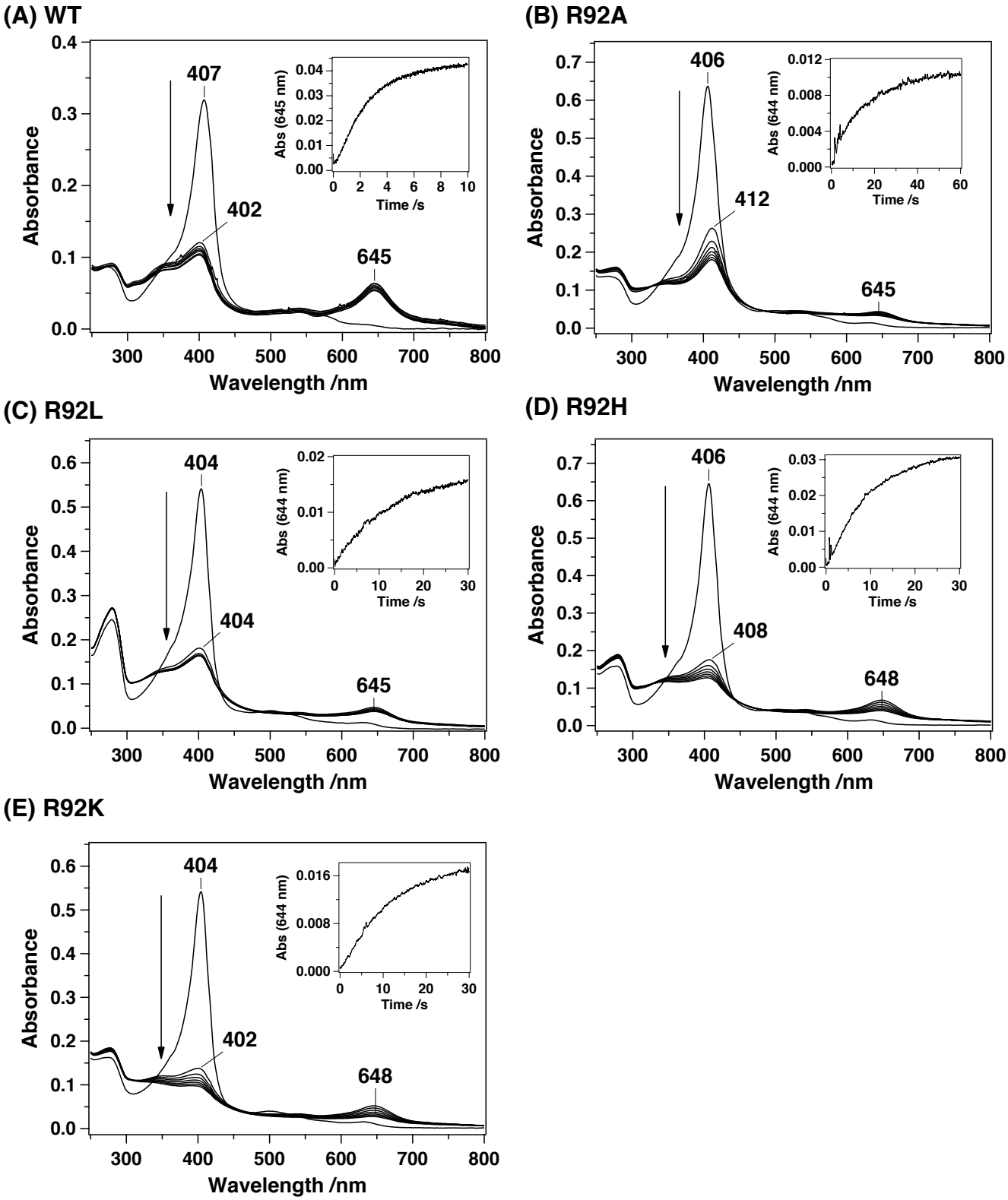

Fig. 7. Heme degradation reaction of the heme-Arg92 HutZ mutants with H_2O_2 (0.2 mM) in 50 mM sodium phosphate and 150 mM NaCl (pH 6.0). Spectra were recorded before the addition of H_2O_2 and at 1-min intervals for 15 min after the addition of ascorbic acid: (A) heme-WT, (B) heme-R92A, (C) heme-R92L, (D) heme-R92H, and (E) heme-R92K. The insets show the time course of absorbance at 644 nm after the addition of H_2O_2 obtained by stopped-flow method.

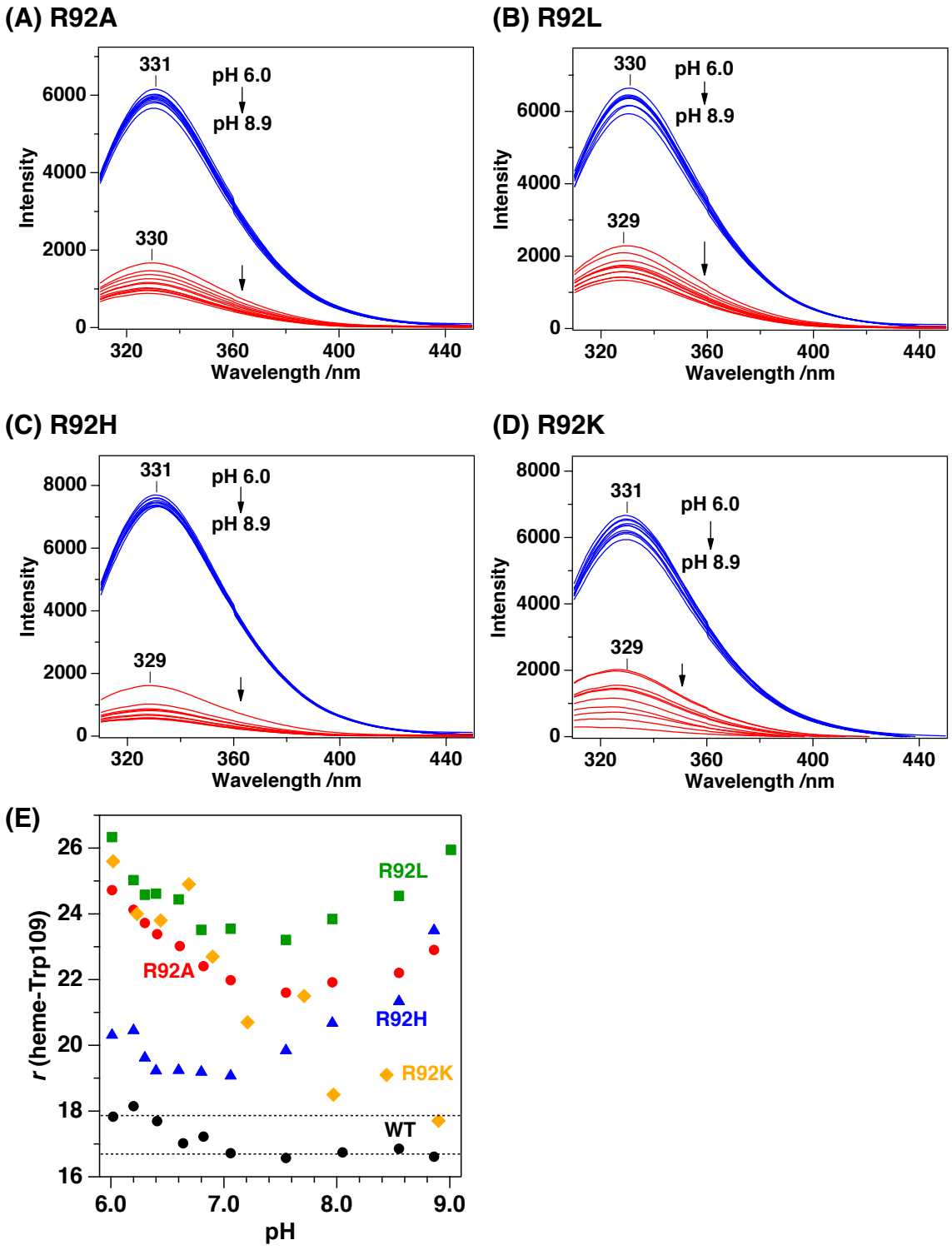

Fig. 8. Fluorescence spectra of the ferric (A) R92A, (B) R92L, (C) R92H and (D) R92K mutant HutZ s in the absence (blue lines) and presence of heme (red lines) at pH 6.0–9.0. Spectra were recorded with excitation at 295 nm. The sample concentration was 3 μM. (E) pH dependence of the distance between heme and Trp109 estimated by quenching of tryptophan fluorescence by energy transfer efficiency and the Förster distance using equation 2.

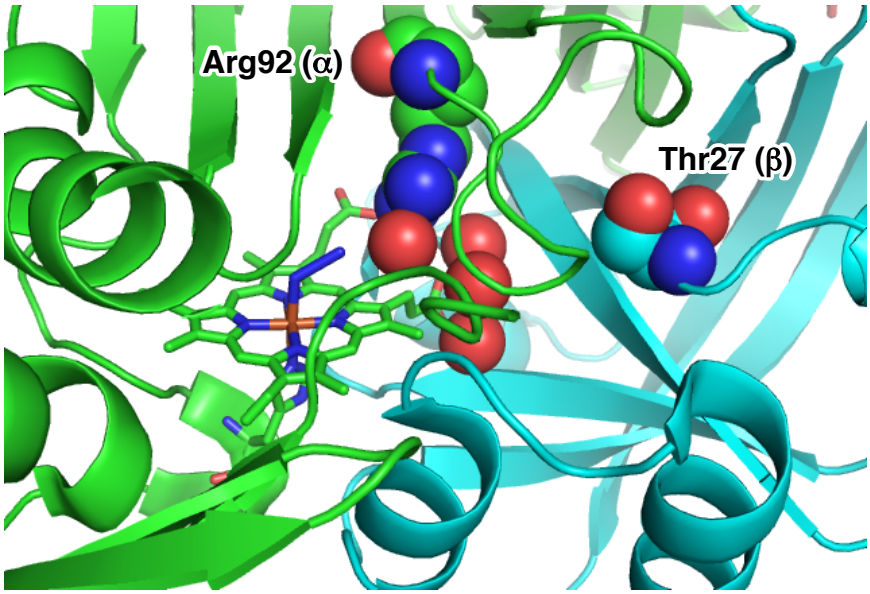

Fig. 9. Crystal structures of a HutZ homologous protein HugZ from *H. pylori* (PDB ID code 3GAS). The residue numbering is based on *V. cholerae* HutZ. A cluster of water molecules is formed between Arg92 and Thr27.

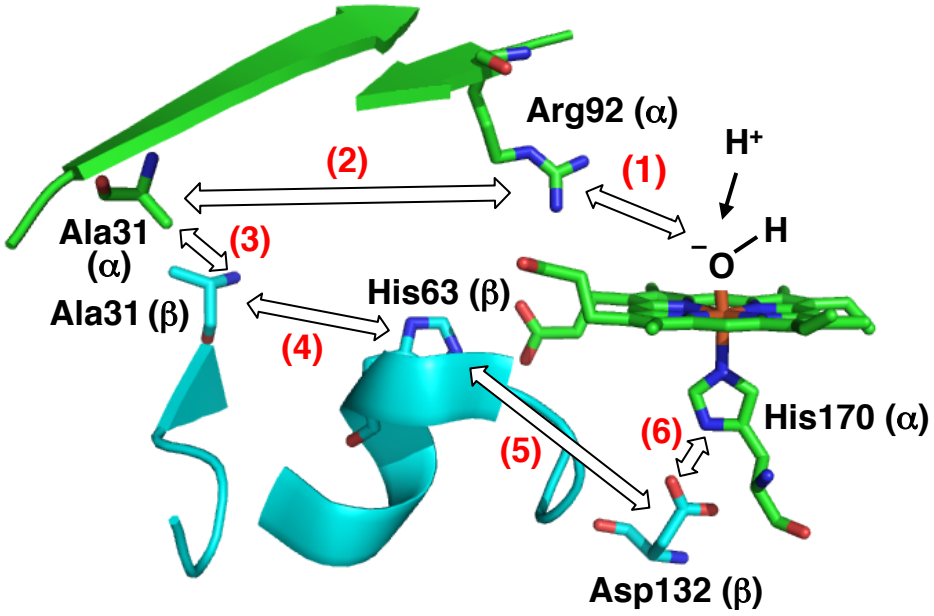

Fig. 10. Proposed regulation mechanism of heme degradation by HutZ *via* subunit-subunit interactions. The numbers show the sequence of events occurred during conversion from inactive to active forms of HutZ.

Supplementary data

Role of conserved arginine in the heme distal site of HutZ from *Vibrio cholerae* in the heme degradation reaction

Takeshi Uchida[*a,b], Nobuhiko Dojun[a], Kazuki Ota[a], Yukari Sekine[a], Yuina Nakamura[a], Sayaka Umetsu[c] and Koichiro Ishimori [a,b]

[a]Department of Chemistry, Faculty of Science, Hokkaido University, Sapporo 060-0810, Japan

[b]Graduate School of Chemical Sciences and Engineering, Hokkaido University, Sapporo 060-8628, Japan

[3]Division of Chemistry, School of Science, Hokkaido University, Sapporo 060-0810, Japan

*Corresponding author: Department of Chemistry, Faculty of Science, Hokkaido University, Sapporo 060-0810, Japan

E-mail address: uchida@sci.hokudai.ac.jp (T. Uchida).

Supplemental Table 1: Oligonucleotides used for construction of expression vectors for mutants. The underlined bases signify the introduced mutations.

Mutants	Primers (up, sense; bottom, anti-sense)
R92A	5'-CGTAAAGCGCTGACCTTTGATGCGGTTG-3'
	5'-GGTCAGCGCTTTACGGGCGAAAAGTTG-3'
R92L	5'-CGTAAACTGCTGACCTTTGATGCGGTTG-3'
	5'-GGTCAGCAGTTTACGGGCGAAAAGTTG-3'
R92H	5'-CGTAAACATCTGACCTTTGATGCGGT-3'
	5'-GGTCAGATGTTTACGGGCGAAAAGTTG-3'
R92K	5'-CGTAAAAAACTGACCTTTGATGCGGT-3'
	5'-GGTCAGTTTTTTACGGGCGAAAAGTTG-3'

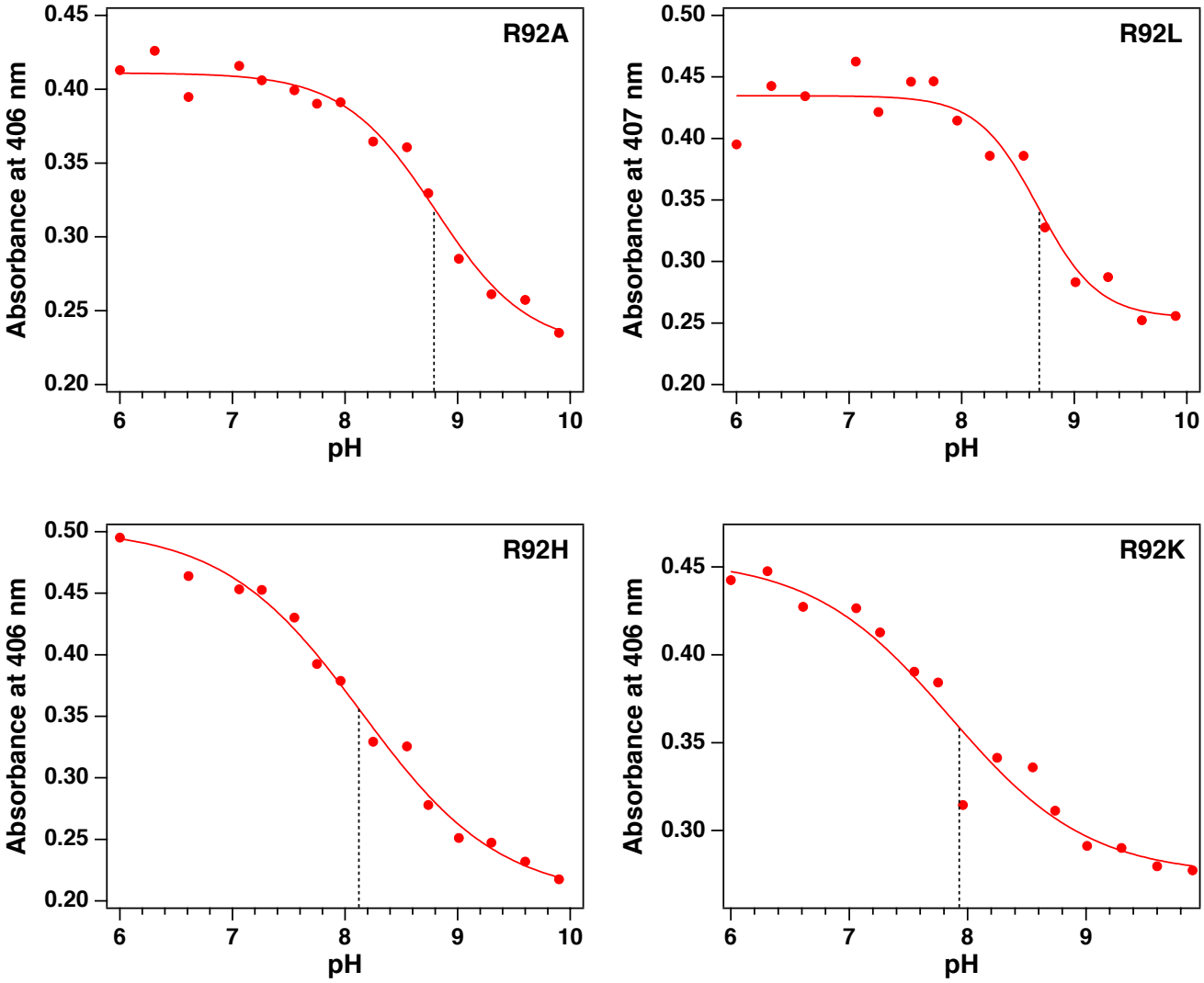

Figure S1. pH dependence of the Soret bands at 406-407 nm for the heme-R92A, heme-R92L, heme-R92H and heme-R92K mutants. The dotted lines show the pK_a value of equilibrium between high-spin and low-spin heme.

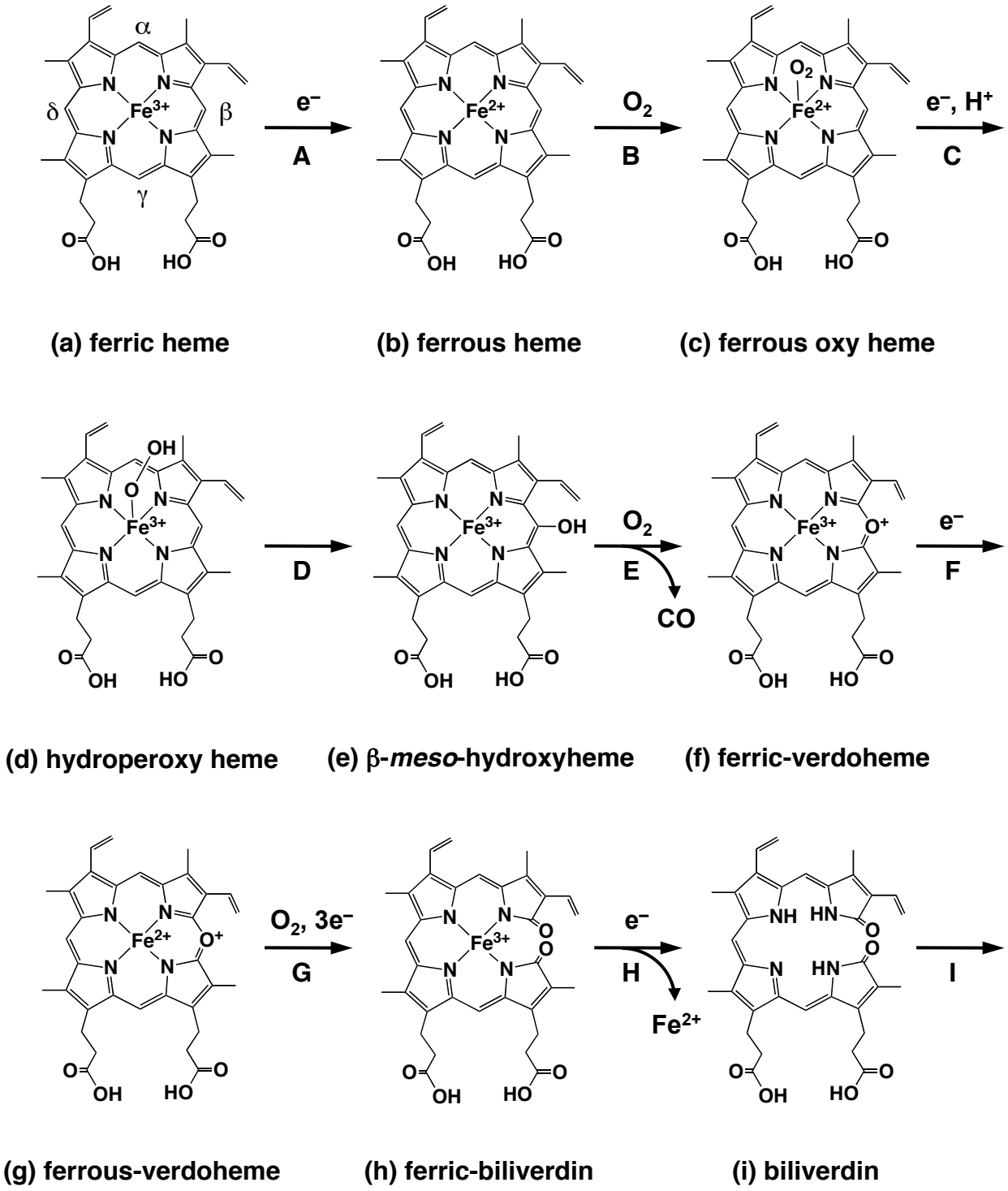

Figure S2. Proposed heme degradation mechanism of HutZ.

Reference Uchida, T., Sekine, Y., Dojun, N., Lewis-Ballester, A., Ishigami, I., Matsui, T., Yeh, S.-R., and Ishimori, K. (2017) Reaction intermediates in the heme degradation reaction by HutZ from *Vibrio cholerae*. *Dalton Trans*. *46*, 8104–8109

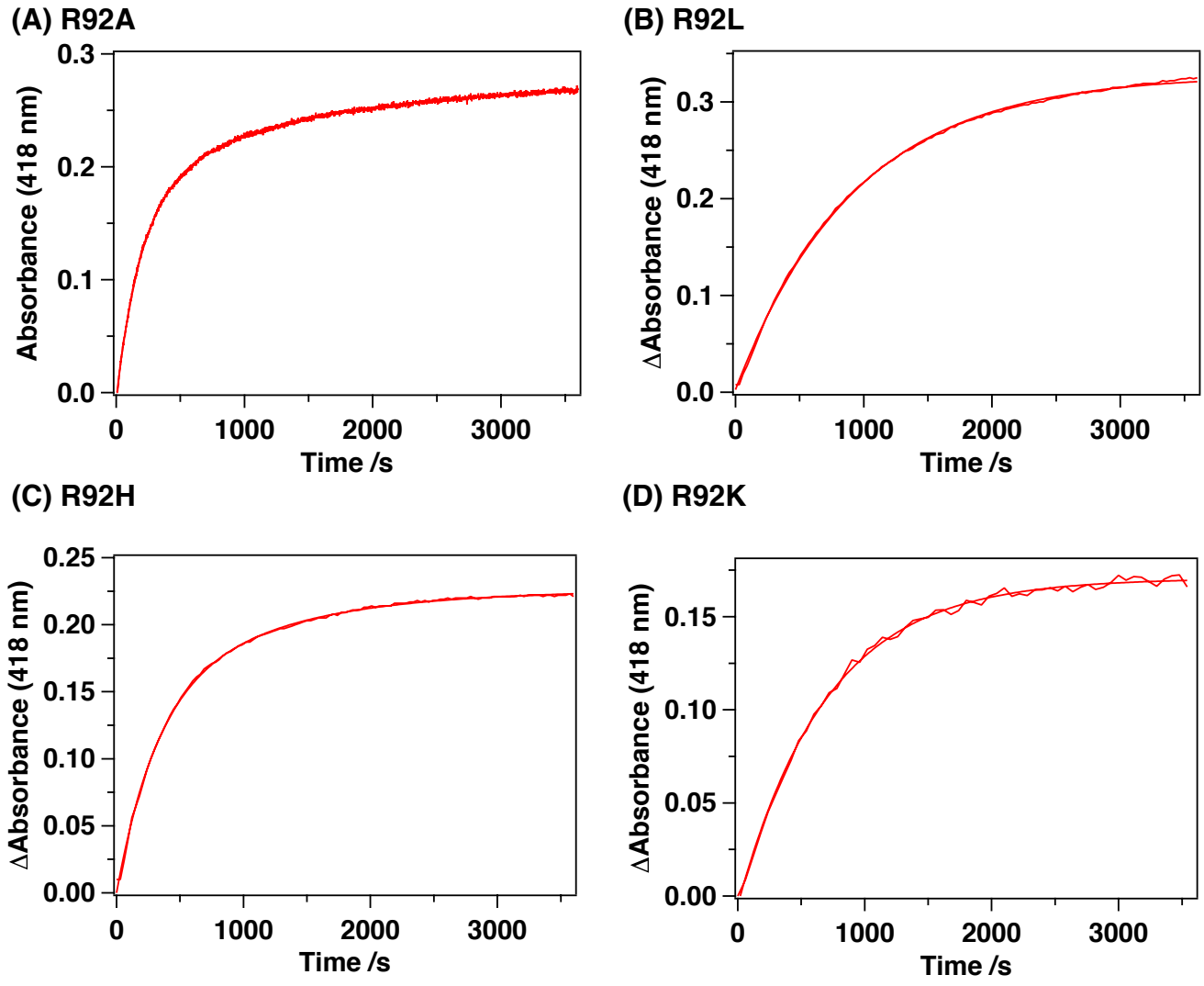

Figure S3. Determination of reduction rates of the ferric heme-Arg92 HutZ mutants. Time course of absorbance changes at 418 nm after the addition of ascorbic acid (final concentration, 1 mM) to ferric heme-HutZ in 50 mM Tris-HCl and 150 mM NaCl (pH 8.0) under a CO atmosphere: (A) heme-R92A, (B) heme-R92L, (C) heme-R92H and (D) heme-R92K.

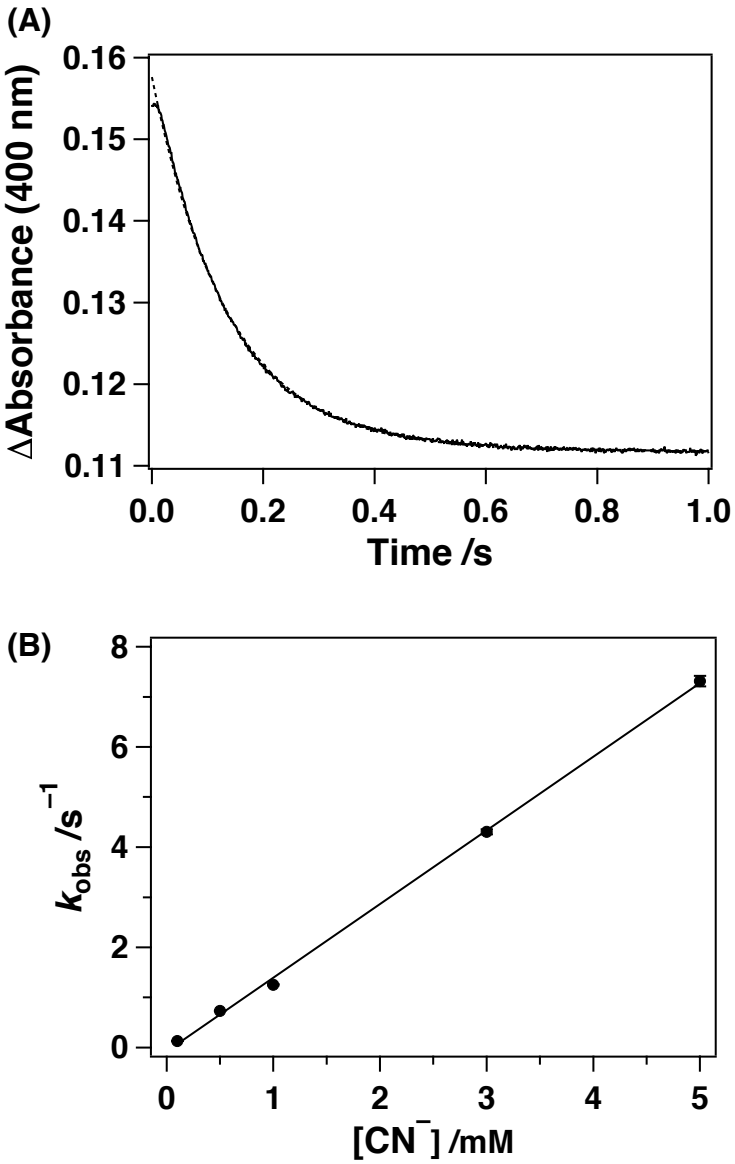

Figure S4. Cyanide binding to the ferric heme-Arg92 HutZ mutants. (A) Typical time course of absorbance changes at 400 nm upon mixing 5 μM protein with 1 mM cyanide in 50 mM Tris-HCl and 150 mM NaCl (pH 8.0). (B) Plots of calculated kobs versus cyanide concentration.

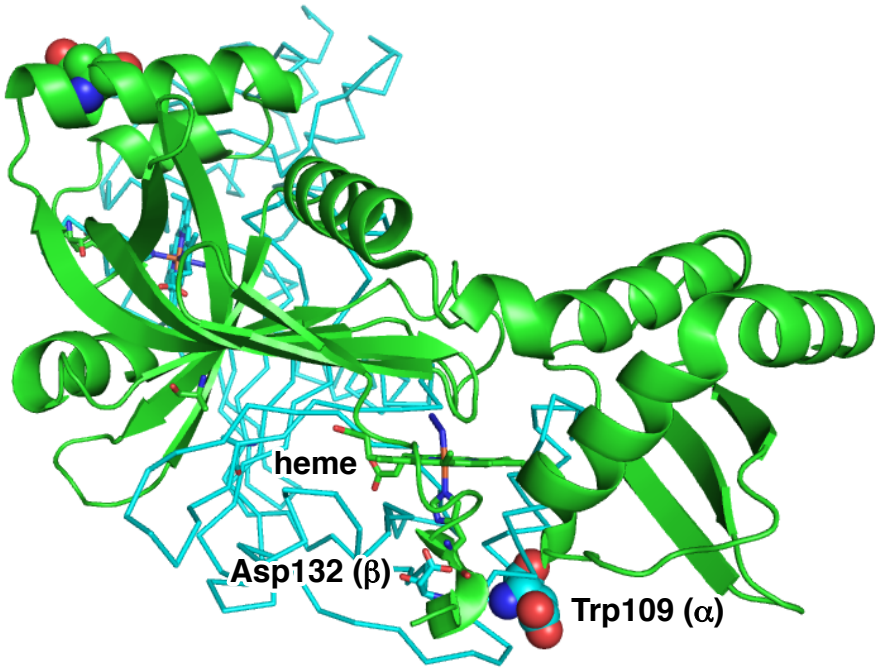

Figure S5. Location of Trp109 and heme on the HugZ crystal structure (PBD ID code 3GAS). Residues are numbered according to the amino acid sequence of HutZ from *V. cholerae*. Green and cyan show each protomer. Trp109 is present in a different protomer (green) from that (cyan) containing nearby Asp132.

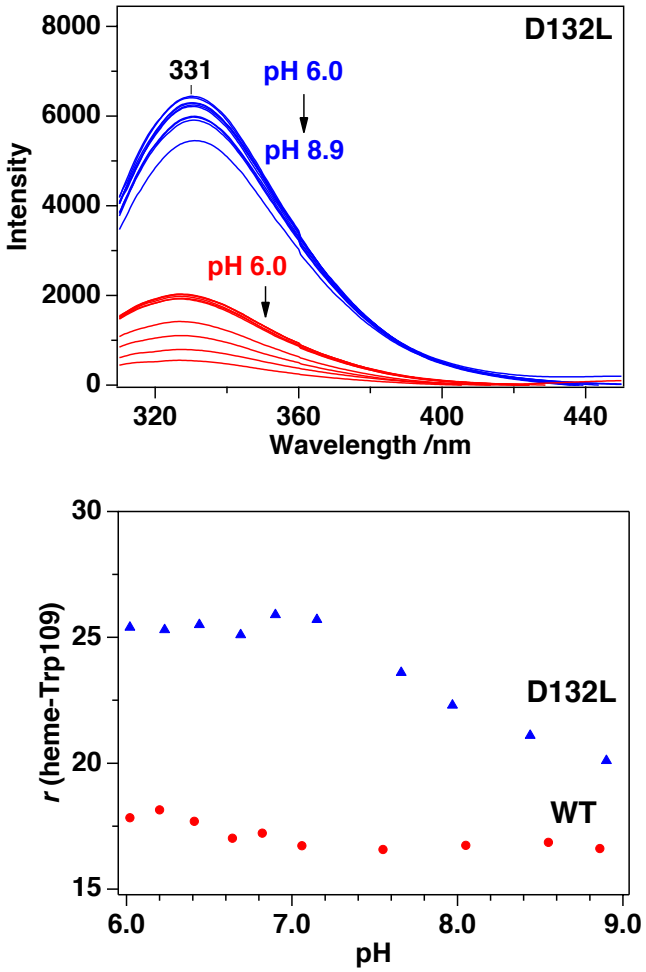

Figure S6. Fluorescence spectra of the ferric D132L HutZ mutants in the absence (blue lines) and presence of heme (red lines) at pH 6.0–9.0. Spectra were recorded with excitation at 295 nm. The sample concentration was 3 μM.

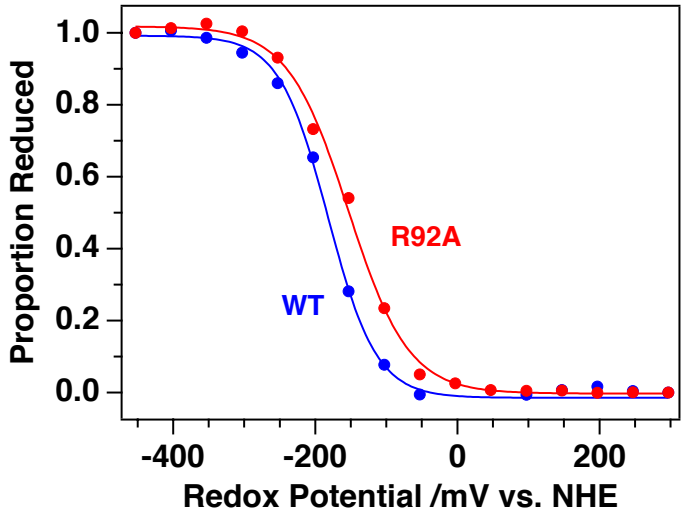

Figure S7. Determination of the reduction potential of heme. Redox titration curve for the heme-HutZ complex monitored by optical spectroscopy at 25 °C; WT (blue line) and R92A mutant (red line). The ratio of reduced to oxidized heme was determined by changes in absorbance at 426 nm. The solid line represents a fit of experimental points to the Nernst equation. Reduction potentials are reported relative to standard hydrogen electrode (SHE). The protein concentration was 30 μM in 50 mM Tris-HCl and 150 mM NaCl (pH 8.0).

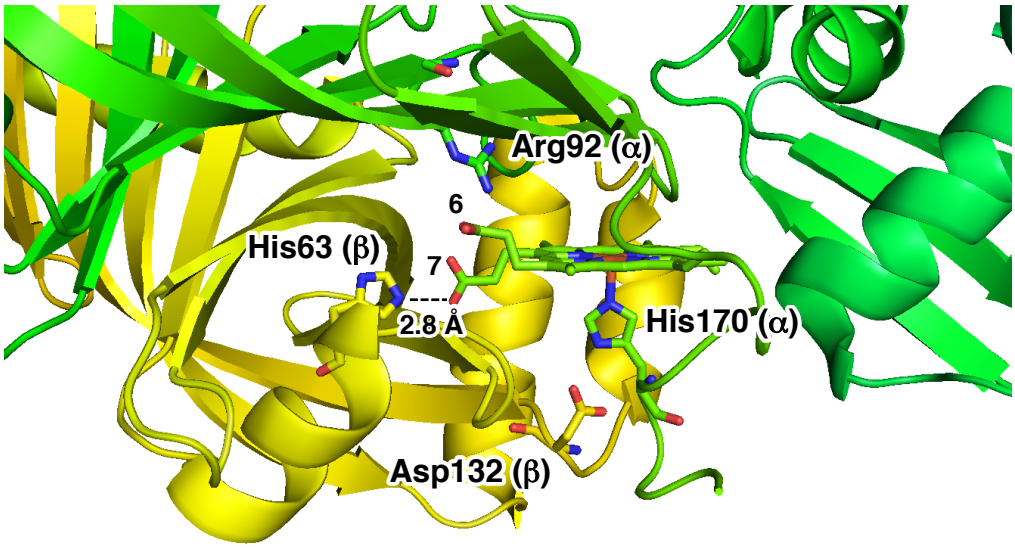

Figure S8. Crystal structure of HugZ from *Helicobacter pylori* (PDB ID code 3GAS). Residues involved in the heme degradation reaction of HutZ are shown. Amino acid residues are numbered according to the sequence of HutZ from *V. cholerae*. α and β indicate the subunits. The number 6 and 7 shows the position of the propionate groups. The nearest distance between His63 and propionate 7 is 2.8 Å.